Evaluation of Creep Models for Soft Soils
(under axially symmetric conditions)

CO-710203/21
september 2001

Evaluation of Creep Models for Soft Soils
(under axially symmetric conditions)

CO-710203/21
september 2001

Client: DELFT CLUSTER
P.O. BOX 69
DELFT

DEPARTMENT OF STRATEGIC RESEARCH
Project manager : dr.ir. E.J. den Haan
Project supervisor : dr.ir. P. van den Berg

GeoDelft
Stieltjesweg 2, 2628 CK DELFT
Postbus 69, 2600 AB DELFT
The Netherlands

Telephone (+31) 15 - 269 35 00
Telefax (+31) 15 - 261 08 21
Postal account 234342
Bank MeesPierson NV
Account 25.92.35.911

Report no.: CO-710203/21	Date report: september 2001
Title and subtitle: Evaluation of Creep Models for Soft Soils (under axially symmetric conditions)	Department: Strategic Research
	Project: Delft Cluster Theme 1 project "Gedrag van Klei en Veen" (Behaviour of Clay and Peat")
Project manager(s): dr.ir. E.J. den Haan	Project supervisor(s): dr.ir. P. van den Berg
Name and address of client: Delft Cluster P.O. Box 69 2600 AB Delft	Reference client: 10203
	Copies sent:
	Type report:

Summary of report:

The *a,b,c* isotache model of MSettle and the Soft Soil Creep Model of Plaxis are subjected to a critical evaluation. These models have not been available for very long, and there is a need to develop an understanding of the strengths and weaknesses of both models. Particular emphasis is placed on the behaviour of the models in the most common axially-symmetric element tests, i.c. the constant rate of strain oedometer test and the various triaxial tests. In a following phase, emphasis could be shifted to applications to practical problems such as embankments.

Both models are briefly described, and earlier work on the properties of the models, parameter determination and parameter correlations is recapitulated. Then, equations are derived which describe stress - strain - strain rate relationships for a number of common element tests such as the Constant Rate of Strain oedometer test, and the various triaxial tests. Some hitherto unknown results are produced from these equation. The equations are applied to tests performed on Dutch clays and peats.

Especial use is made of the K_o-C.R.S. oedometer which is a constant rate of strain oedometer in which lateral stress is also measured. The complete stress state is therefore known, and this creates possibilities for interpretation of the test not only in the 1-D isotache model but also in the 2-D generalized model. This apparatus is quite new and the determination of basic properties such as vertical and horizontal effective stresses, pore pressure etc is given due attention in a separate report ("Interpretatie meetdata en parameterbepaling, K_o-C.R.S. proef", CO-710203/22, september 2001), together with the parameter determination from the test.

Comments:

Keywords: soft soils, organic soils, creep, triaxial test, oedometer test, C.R.S. test, K_o-oedometer test, Oostvaardersplassen clay	Distribution: Assessment team "Gedrag Klei en Veen" (Verruijt, Magnan, H.L. Bakker, A. Nooy van der Kolff) Plaxis: Brinkgreve

Saved:
Title: Evaluation of Creep Models for Soft Soils.doc

No. of pages: 39

Version:	Date:	Prepared by:	Signature:	Checked by:	Signature:
1	september 2001	den Haan		van den Berg	

TABLE OF CONTENTS

1 Introduction

Soft soils in the Netherlands are often not only very compressible, but also have a strong creep tendency. Dutch soil mechanics has always been characterized by its interest in creep phenomena. Keverling Buisman observed and modelled creep settlements before 1936, and Koppejan produced an adaptation to this model which is still in use today. The *a,b,c* isotache model was introduced in 1994 and is currently implemented in the GeoDelft settlement program MSettle. It is an updated approach to creep based on a unique relationship between vertical effective stress, acquired strain and rate of creep strain. In MSettle, the model is applied to 1-D settlement of 1-D or 2-D load configurations (fills, embankments, footings etc). The finite element code Plaxis has an option for a creep model for soft soils which is basically a generalization to 2-D of the *a,b,c* isotache model.

The Plaxis soft soil creep model and the MSettle *a,b,c* isotache model are gradually finding use in engineering practice. A thorough analysis of these models will be of help to this process, by pinpointing strengths and weaknesses of the models. Parameter determination from laboratory tests and correlations of parameters with general soil properties will also be helpful is this respect. The present study aims at contributing to these needs.

Both models are briefly described, and earlier work on the properties of the models, parameter determination and parameter correlations is recapitulated. Then, equations are derived which describe stress - strain - strain rate relationships for a number of common element tests such as the Constant Rate of Strain oedometer test, and the various triaxial tests. These are applied to tests performed on Dutch clays and peats. A number of hitherto unknown features of the models are revealed by these equations.

Especial use is made of the K_o-C.R.S. oedometer which is a constant rate of strain oedometer in which lateral stress is also measured. It was developed by GeoDelft, originally for the Technische Adviescommissie voor de Waterkeringen T.A.W., and later improved for Delft Cluster as part of the project "Gedrag Klei en Veen". By measuring the lateral stress, the complete stress state is known, and this creates possibilities for interpretation of the test not only in the 1-D isotache model but also in the 2-D generalized model. This apparatus is quite new and the determination of basic properties such as vertical and horizontal effective stresses, pore pressure etc is given due attention in a separate report ("Interpretatie meetdata en parameterbepaling, K_o-C.R.S. proef", CO-710203/22, september 2001), together with the parameter determination from the test.

In a following phase of the study, Plaxis could be applied to a simple embankment geometry to study parameter sensitivity of a number of important parameters.

2 General equations

General definitions and equations which form the basis of the report are given below.
Where axially-symmetric stress and strain conditions occur, the major and minor principal directions are denoted by the indices 1 and 3 resp. The subscripts $_v$ and $_s$ denote volumetric (isotropic) and shear (deviatoric) conditions resp. The superscripts ^{d} and ^{s} denote direct (elastic) and secular (creep) components of strain. All strains are logarithmic, natural strains.

$$\begin{aligned} p' &= \frac{s'_1 + 2s'_3}{3} \\ q &= s'_1 - s'_3 \end{aligned} \tag{2.1}$$

$$e_1^d = \frac{s'_1}{E} - 2\nu\frac{s'_3}{E} = \frac{p' + \frac{2}{3}q - 2\nu\,(p' - \frac{1}{3}q)}{E} = \frac{p'(1-2\nu) + \frac{2}{3}q(1+\nu)}{E} \tag{2.2}$$

$$e_3^d = -\nu\frac{s'_1}{E} + (1-\nu)\frac{s'_3}{E} = \frac{-\nu(p' + \frac{2}{3}q) + (1-\nu)(p' - \frac{1}{3}q)}{E} = \frac{p'(1-2\nu) - \frac{1}{3}q(1+\nu)}{E} \tag{2.3}$$

$$\begin{aligned} s'_1 &= p' + \tfrac{2}{3}q \\ s'_3 &= p' - \tfrac{1}{3}q \end{aligned} \tag{2.4}$$

$$\begin{aligned} e_v &= e_1 + 2e_3 & e_1 &= \tfrac{1}{3}e_v + e_s = e_v(\tfrac{1}{3} + e_s/e_v) \\ e_s &= \tfrac{2}{3}(e_1 - e_3) & e_3 &= \tfrac{1}{3}e_v - \tfrac{1}{2}e_s = e_v(\tfrac{1}{3} - e_s/2e_v) \end{aligned} \tag{2.5}$$

Incrementally:

$$\dot{\varepsilon}_v^d = a\,(\ln \dot{p}') = a\,\frac{\dot{p}'}{p'} \tag{2.6}$$

$$E = 3K(1-2\nu) = \frac{3}{k}p'(1-2\nu) \tag{2.7}$$

$$\dot{p}' = \frac{p'}{k}\dot{\varepsilon}_v^d \tag{2.8}$$

$$\begin{aligned} \dot{q} &= 2G(\dot{\varepsilon}_1^d - \dot{\varepsilon}_3^d) = \frac{E}{(1+\nu)}(\dot{\varepsilon}_1^d - \dot{\varepsilon}_3^d) \\ &= \frac{E}{(1+\nu)}(\dot{\varepsilon}_1^d - \dot{\varepsilon}_3^d) = \frac{3p'(1-2\nu)}{a\,(1+\nu)}(\dot{\varepsilon}_1^d - \dot{\varepsilon}_3^d) \\ &= \frac{p'}{a\,b}(\dot{\varepsilon}_1^d - \dot{\varepsilon}_3^d) \qquad \text{with} \quad b = \frac{1+\nu}{3(1-2\nu)} \end{aligned} \tag{2.9}$$

$$\dot{\varepsilon}_1^d - \dot{\varepsilon}_3^d = \frac{a\,(1+\nu)}{3(1-2\nu)}\frac{\dot{q}}{p'} = a\,b\,\frac{\dot{q}}{p'} \tag{2.10}$$

$$\varepsilon_1^d = \frac{\Delta\sigma'(1-2\nu) + \frac{2}{3}\Delta q(1+\nu)}{E} = \frac{a}{3}\frac{\Delta\sigma'}{\sigma'}\left(1+2b\frac{\Delta q}{\Delta\sigma'}\right) \quad (2.11)$$

$$\varepsilon_3^d = \frac{\Delta\sigma'(1-2\nu) - \frac{1}{3}\Delta q(1+\nu)}{E} = \frac{a}{3}\frac{\Delta\sigma'}{\sigma'}\left(1-b\frac{\Delta q}{\Delta\sigma'}\right) \quad (2.12)$$

$$K_o = \frac{\sigma_3'}{\sigma_1'} = \frac{1-\frac{q}{3\sigma'}}{1+\frac{2q}{3\sigma'}} = \frac{3-\frac{q}{\sigma'}}{3+2\frac{q}{\sigma'}} = \frac{3-h_{Ko}}{3+2h_{Ko}} \quad \text{with } h_{Ko} = \frac{q}{\sigma'} \text{ in the 1-D state} \quad (2.13)$$

$$h_{Ko} = 3\frac{1-K_o}{1+2K_o} \quad (2.14)$$

3 The *a,b,c* Isotache model

3.1 Model description

The *a,b,c* isotache model was developed as an alternative to the Buisman/Koppejan compression model. The latter is defective in a number of respects, the most serious of which are the erroneous superposition principle introduced by Keverling Buisman (as a preliminary assumption which he stressed needed confirmation), and the lack of clarity regarding the origin of time in describing creep. The model is described fully in Den Haan (1994, 1996, 2000, 2001).

In the *abc* model, total rate of strain is obtained by adding the direct ("elastic") rate of strain and the secular (creep or "viscoplastic") rate of strain. These latter are obtained from constitutive equations containing present strain, effective vertical stress, and the rate of change of the latter. A compression calculation proceeds incrementally in time by multiplying the total rate of strain with the increment of time which gives the increment of compression.

The terms "direct" and "secular" may sound new and unusual, but in fact they have historical justification. Keverling Buisman introduced them in 1936, much earlier than terms such as "instant" and "delayed" which imply exactly the same. Terms such as "elastic" and "visco-plastic" are also in use.

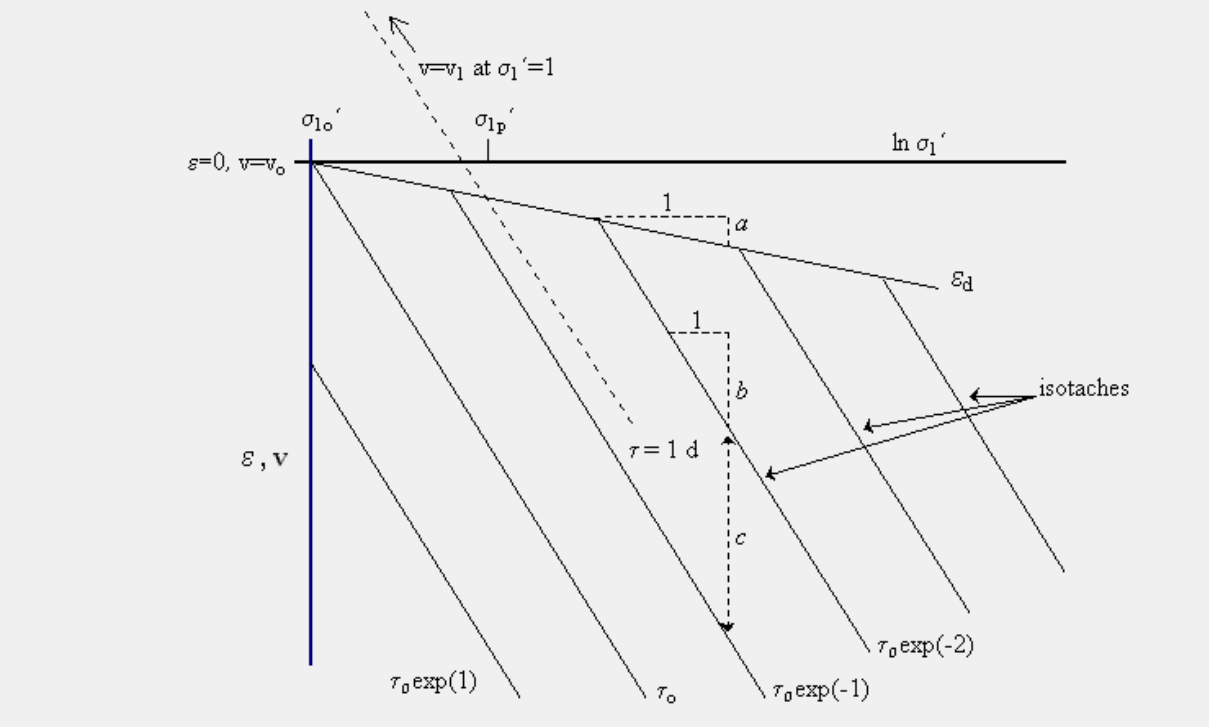

The figure illustrates the model. Direct strain e_d occurs due to increase of effective vertical stress s_1'. A conventional strain-log(stress) relationship describes this:

$$e_d = a\ln(s_1' / s_{1o}') \tag{3.1}$$

and

$$\dot{e}_d = a\dot{s}_1' / s_1' \tag{3.2}$$

with *a* being the direct compression index.

The series of parallel lines in the figure are creep isotaches. They are given by

$$e = b\ln(s_1' / s_{1o}') + c\ln(t / t_o) \tag{3.3}$$

where *b* is the secular compression index and *c* is the coefficient of rate of secular compression. The *intrinsic time* τ is related to secular strain rate $\dot{e}_s$ by

$$\dot{e}_s = c / t \tag{3.4}$$

Any given combination of ε, $\sigma'_{,1}$ and τ is unique. That is, given stress and strain, then secular strain rate is known. The initial conditions are denoted by an subscript o. The relation between true time t and τ is given by

$$t = t_r + t \tag{3.5}$$

Time t can be measured from any origin, e.g. years A.D. (Keverling Buisman), start of construction, start of the stage, etc, and t_r changes accordingly. Intrinsic time τ is insensitive to changes in the origin of t, and remains related to creep isotaches as shown in the figure. At constant vertical effective stress, the figure and the equation of the isotaches reveal a linear relationship between strain and log *t*. This is slightly different than the conventional strain - log *t* relationship. *t* is the geological time necessary to attain the present degree of compression under the present vertical effective stress, if that stress was applied at the moment of formation of the soil. We may therefore expect that τ_o is related to the geological age of the soil, although the sheer magnitude of the time involved will have induced

changes in the soil not covered by the present configuration of the isotaches, thereby preventing simply equating the two.

When t_r is small relative to τ, then $t \approx \tau$ and a linear semi-log plot is obtained for both t and τ. This is the case at large values of t, and the asymptote of the ε - log t curve is identical to the ε - log t relationship for a constant s'_1. If a large load increment is applied, a large excursion is made to the right in the figure, and low values of τ occur. t_r is then almost zero if time t is measured from the moment of load application. Then $t \approx \tau$, and this remains the case during the subsequent creep at constant s'_1. This is the normal case with a Load-Increment-Ratio of 1 in incremental loading oedometer tests. The applied load increment is large relative to the existing load, and the intrinsic time becomes low. Memory is wiped out as it were.

There exists an isotache on which τ = 1 day. Creep rate $\dot{\varepsilon}_s = c\ [1/day]$ on this isotache. Rate of strain in conventional incremental loading oedometer tests is approximately also equal to c [1/day], and the intersection of this isotache with the direct strain line through the initial condition yields a stress which approximates the preconsolidation pressure s'_{1p}.

The expression for $\dot{\varepsilon}_s$ can be elaborated in several ways by expressing τ as a function of various parameters and state variables. For example:

$$\begin{aligned}
\dot{\varepsilon}_s &= \frac{c}{t_o} e^{-e/c} \left(\frac{s'_1}{s'_{1o}} \right)^{b/c} = \frac{c}{t_R} e^{-(e-e_R)/c} \left(\frac{s'_1}{s'_{1R}} \right)^{b/c} \\
&= \frac{c}{t_1} e^{-e/c} \left(\frac{s'_{1o}}{s'_{1p}} \right)^{(b-a)/c} \left(\frac{s'_1}{s'_{1o}} \right)^{b/c} = \frac{c}{t_R} e^{-(e_s - e_{s,R})/c} \left(\frac{s'_1}{s'_{1R}} \right)^{(b-a)/c} \\
&= \frac{c}{t_1} e^{-e_s/c} \left(\frac{s'_1}{s'_{1p}} \right)^{(b-a)/c} = \frac{c}{t_o} e^{-e_s/c} \left(\frac{s'_1}{s'_{1o}} \right)^{(b-a)/c} \\
&= \frac{c}{t_1} \left(\frac{s'_1}{s'_{1c}} \right)^{(b-a)/c}
\end{aligned} \tag{3.6}$$

in which

$$s'_{1c} = s'_{1p} e^{-e_s/(b-a)} \tag{3.7}$$

The compression in a time step can only occur if pore water flows out. The rate of compression due to outflow $\dot{\varepsilon}_q$ of course equals the total rate of strain. We equate this to the sum of the direct and secular rates, giving

$$\dot{\varepsilon}_q = \dot{\varepsilon}_d + \dot{\varepsilon}_x \tag{3.8}$$

$\dot{\varepsilon}_q$ is controlled by Darcy's law and the above equation can be expanded into the "finite strain consolidation equation". It automatically yields the development of excess pore pressures during consolidation, as well as the development of strains. Self-weight effects are included.

If for example secular strain rate is high due to a strong creep potential, and outflow is slow due to low permeability, it may occur that pore pressures increase rather than decrease. This is a fundamental difference with Terzaghi consolidation.

A simple p.c. program named Consef is available to aid in understanding the *a,b,c* isotache model. See Den Haan (2001). Consef stands for consolidation and secular effect. It determines strains due to 1d stage loading of a multi-layered soft saturated soil. A description of the model and the program is given, and worked examples and exercises are included.

3.2 Natural strain

The *a,b,c* model works with natural strain. This is the preferred measure of strain for soft soils. These soils stiffen strongly as compression increases, and the C_c parameter based on linear strain is not able to describe this. The various material models of Plaxis, including those for soft soils, use linear strain, and this is a disadvantage. The usual approximation in small strain models:

$$e_v = e_1 + 2e_3 \tag{3.9}$$

becomes erroneous at large strain if linear strain is used, but remains correct if natural strain is used.

In this report, natural strain will be used. It is represented as ε. This differs from other descriptions of the *a,b,c* model, in which natural strain is represented as ε^H where the superscript refers to Hencky to whom its first usage is ascribed.

3.3 Correlations

Correlations of b with liquid limit and plasticity index for clay and with loss-on-ignition (roughly equivalent to organic content) for peat are given in Den Haan (1992). A correlation of b with bulk density for clay and peat is given in Den Haan & Sellmeijer (2000) as $b \approx 0.326(\gamma_{tot}/\gamma_{water})^{-2.11}$ and shown in the following figure. When applying this correlation to peat, the bulk density to be used is that as measured in the laboratory after sampling and attendent loss of pore water from coarse-fibrous peat. This explains the values of specific bulk density below 1. The correlation is not suitable for pure peats with a low von Post number (low degree of humification), but such peat is not common in the Netherlands.

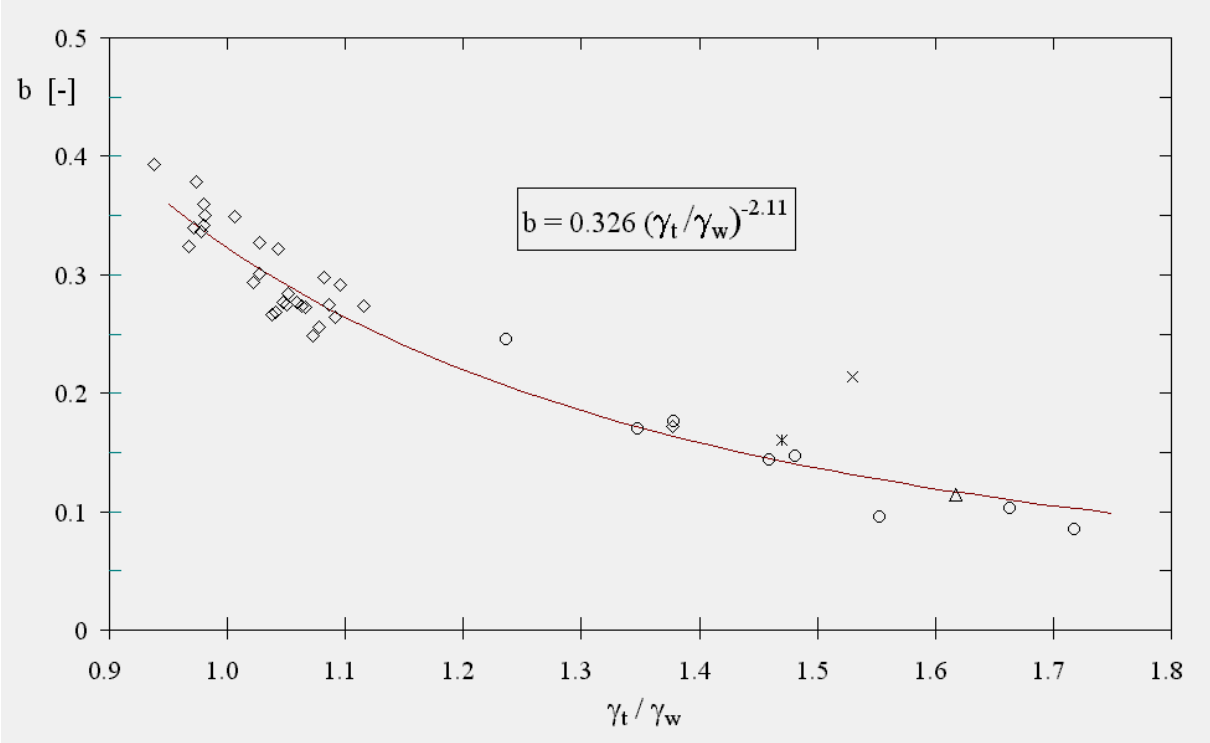

Interrelationships of the other parameters with b can be assumed. Reasonable values are $v_1=40b$, $a=0.1b$, $c=0.04b$.
$\tau_o \approx 10^3$ - 10^4 [days] for soft soil.

4 The Natural Strain - Soft Soil - Creep Model

Plaxis has implemented what is essentially a 2-D generalization of the *a,b,c* isotache model. It has been named the "Soft Soil Creep Model". It is cast in terms of linear strain, with parameters κ^*, λ^* and μ^* playing the role of *a, b* and *c* resp. However, it is a wrong choice to write models especially for soft soils and then not to adopt natural strain. It is easier to formulate large strain soil behaviour with natural strain, and the relationship between volume strains and normal strains remains mathematically correct. For this reason, this report will use the *a,b,c* parameters rather than the Plaxis parameters.

The equations given in this section are essentially similar to those derived earlier by Fokker (1996) and by Plaxis in its Materials Manual. A completely similar model was presented earlier by Kutter and Sathialingam (1992).
The figures above illustrate the model. In q,p space the Modified Camclay yield surface is replaced by

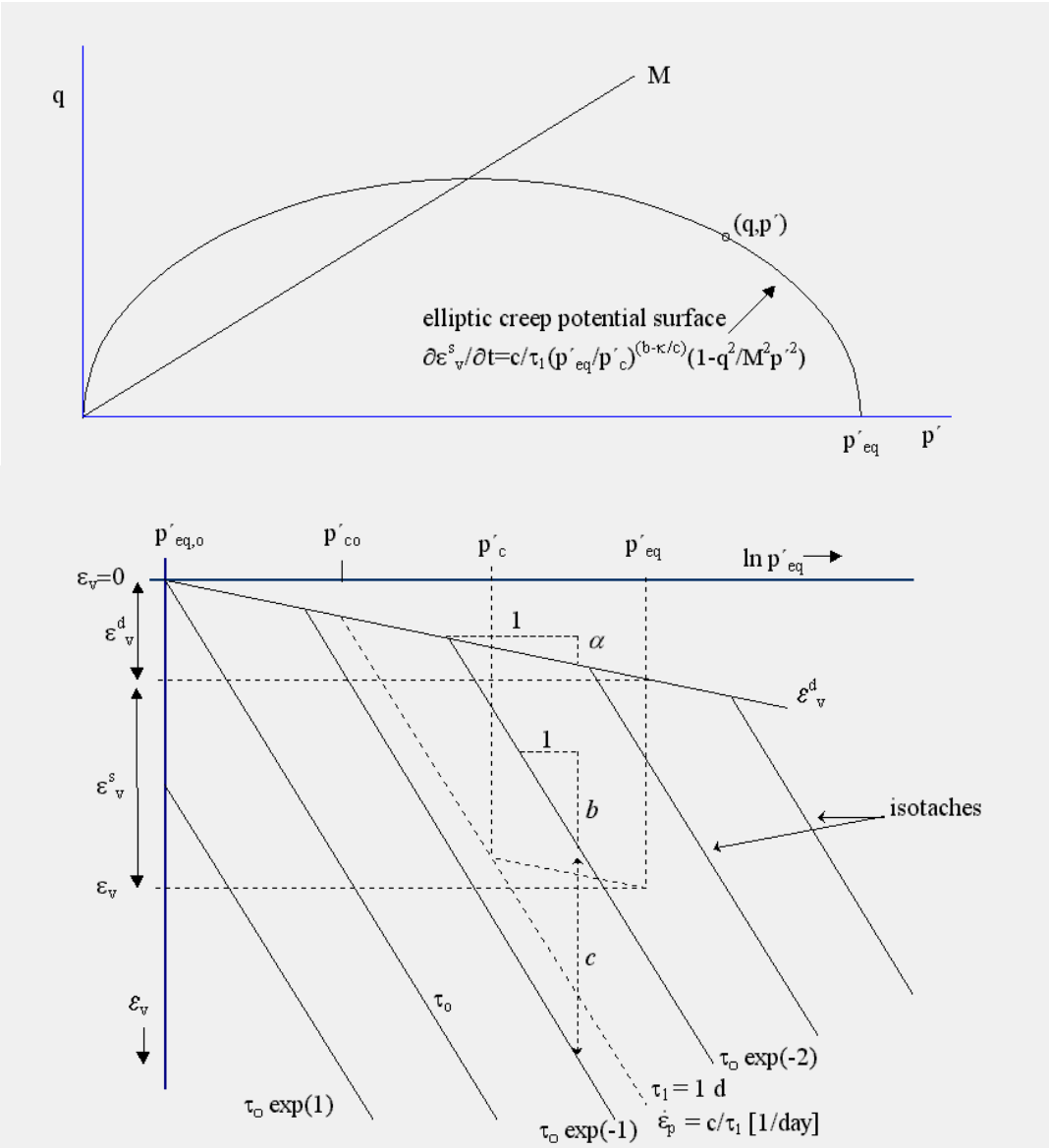

a creep potential surface of the same elliptic shape, which determines the volumetric creep rate of strain for all stress points on it. The ellipse is characterized by its intersection p'_{eq} with the isotropic

axis, and the apex ratio of q /p´ = M. Volumetric creep strain increments are determined from p'_{eq} in the isotache plane, and the shear creep strain increment follows from this through the normality condition on the potential surface.
The equivalent stress p'_{eq} is found from the acting stresses q , p by the ellipse passing through both states. The ellipse is given by

$$p'^2 + \frac{q^2}{M^2} = p'_{eq}\, p' \tag{4.1}$$

so p'_{eq} can be calculated for any given state of stress.

In the isotache plane, volumetric strain ε_v is plotted against equivalent isotropic stress p'_{eq} . The direct strains are now given by a slope a , but the slope and spacing of the creep isotaches remain at b and c as in the 1-D model. a is related to a by (see Plaxis (1998))

$$a = \frac{a}{1+2K_o}\frac{1+n}{1-n} \tag{4.2}$$

For stress states which are not linear relative to the stress origin, a and a do not have a simple interrelationship. A common assumption is to take K_o=1 so that

$$\frac{a}{a} = \frac{3(1-n)}{(1+n)} \tag{4.3}$$

The isotache with intrinsic time τ_1=1day corresponds to the initial preconsolidation pressure p'_{co} for zero secular strain. Under a state of arbitrary equivalent stress p'_{eq} and secular strain e_v^s an updated value of the preconsolidation pressure p'_c is given by

$$p'_c = p'_{co} \exp(e_v^s /(b-a)) \tag{4.4}$$

p'_{co} also provides a link between the initial intrinsic time τ_o and τ_1 :

$$t_o = t_1 \left(\frac{p'_{co}}{p'_{eq,o}} \right)^{\frac{b-a}{c}} \tag{4.5}$$

The current intrinsic time is given by

$$t = t_1 \left(\frac{p'_c}{p'_{eq}} \right)^{\frac{b-a}{c}} \tag{4.6}$$

and current rate of volumetric creep strain follows from this simply by

$$\dot{\varepsilon}_v^s = c/t = \frac{c}{t_1}\left(\frac{p'_{eq}}{p'_c} \right)^{\frac{b-a}{c}} \tag{4.7}$$

This rate applies when stresses are isotropic. In the presence of a deviatoric stress, the rate is modified. Generally, secular strain rate is obtained from the plastic potential surface by the equation

$$\dot{\varepsilon}_{ij}^{\,s} = \frac{c}{t_1}\left(\frac{p_{eq}}{p_c} \right)^{\frac{b-a}{c}} \frac{\partial p_{eq}}{\partial s'_{ij}} \tag{4.8}$$

It can be derived from this that

$$\dot{\varepsilon}_v^s = c/t = \frac{c}{t_1}\left(\frac{p'_{eq}}{p'_c} \right)^{\frac{b-a}{c}} \left(1 - \frac{q^2}{p'^2 M^2} \right) = \frac{c}{t_1}\left(\frac{p'_{eq}}{p'_c} \right)^{\frac{b-a}{c}} \left(\frac{M^2 - h^2}{M^2} \right) \tag{4.9}$$

The preceding equation is a result of the choice of the Modified Camclay ellipse as the plastic potential. The last factor on the r.h.s. expresses the derivative of the surface to the volumetric stress.

Secular strain rates in the normal directions can also be obtained from (4.8), as well as the secular rate of shear strain. Knowing the rate of volumetric creep strain, the rate of shear strain can also be found from the normality condition of the potential surface

$$\frac{\dot{\varepsilon}_s^s}{\dot{\varepsilon}_v^s} = \frac{-dp'}{dq} = \frac{q}{M^2(p' - \tfrac{1}{2}\, p'_{eq})} = \frac{2qp'}{M^2 p'^2 - q^2} = \frac{2h}{M^2 - h^2} \tag{4.10}$$

$$\dot{\varepsilon}_s^s = \frac{c}{t_1}\left(\frac{p'_{eq}}{p'_c}\right)^{\frac{b-a}{c}} \frac{2h}{M^2} \tag{4.11}$$

where $\eta = q / p'$ is the mobilized shear stress ratio. The creep strain rates in the two normal directions are then obtained as follows:

$$e_1 = \tfrac{1}{3} e_v + e_s = e_v(\tfrac{1}{3} + e_s / e_v)$$

from which follows

$$\begin{aligned} \dot{\varepsilon}_1^s &= \dot{\varepsilon}_v^s(\tfrac{1}{3} + \frac{\dot{\varepsilon}_s^s}{\dot{\varepsilon}_v^s}) \\ &= \frac{c}{t_1}\left(\frac{p'_{eq}}{p'_c}\right)^{\frac{b-a}{c}} \left(1 - \frac{q^2}{p'^2 M^2}\right)\left(\tfrac{1}{3} + \frac{2qp'}{M^2 p'^2 - q^2}\right) \\ &= \frac{c}{3t_1}\left(\frac{p'_{eq}}{p'_c}\right)^{\frac{b-a}{c}} \left(1 - \frac{q^2 - 6qp'}{p'^2 M^2}\right) = \frac{c}{3t_1}\left(\frac{p'_{eq}}{p'_c}\right)^{\frac{b-a}{c}} \left(1 - \frac{h^2 - 6h}{M^2}\right) \end{aligned} \tag{4.12}$$

and

$$e_3 = \tfrac{1}{3} e_v - \tfrac{1}{2} e_s = e_v(\tfrac{1}{3} - e_s / 2e_v)$$

from which follows

$$\begin{aligned} \dot{\varepsilon}_3^s &= \dot{\varepsilon}_v^s(\tfrac{1}{3} - \frac{\dot{\varepsilon}_s^s}{2\dot{\varepsilon}_v^s}) \\ &= \frac{c}{t_1}\left(\frac{p'_{eq}}{p'_c}\right)^{\frac{b-a}{c}} \left(1 - \frac{q^2}{p'^2 M^2}\right)\left(\tfrac{1}{3} - \tfrac{1}{2}\frac{2qp'}{M^2 p'^2 - q^2}\right) \\ &= \frac{c}{3t_1}\left(\frac{p'_{eq}}{p'_c}\right)^{\frac{b-a}{c}} \left(1 - \frac{q^2 + 3qp'}{p'^2 M^2}\right) = \frac{c}{3t_1}\left(\frac{p'_{eq}}{p'_c}\right)^{\frac{b-a}{c}} \left(1 - \frac{h^2 + 3h}{M^2}\right) \end{aligned} \tag{4.13}$$

To the creep strain increments are added the direct strain increments as given in the introductory chapter. A number of common laboratory tests can now be solved incrementally on the basis of the preceding equations.

5 Spreadsheet for calculating stresses from strain history

Various laboratory tests apply constant rates of strain to the boundaries of a soil sample. The shear stage of an undrained triaxial test e.g. is usually strain-rate controlled in the vertical direction, and the zero volume change condition produces a constant rate of strain in the lateral direction as well. The oedometer test can be performed under constant rate of vertical strain, with lateral strain being always zero. It is possible to study the effects of various applied rates of vertical and lateral strain in the soft soil creep models. The procedure is given below. It can easily be implemented in a spreadsheet, so as to incrementally determine stresses from the strain history.

***a,b,c* isotache model**

Necessary parameters: *a,b,c*

Initial state: s'_{vo} and s'_{vp} . Strains zero.

Test condition: $d\varepsilon_1/dt$

A series of time steps Δt is defined. For each time step the following steps are performed sequentially:

s'_{vc} is determined from (3.7).

Strains are found from the applied rates and the time step Δt.

Incremental secular vertical strain is found from (3.6) and the time step Δt.

Incremental vertical stress is found from (3.2)

Stresses and strains are updated by adding the calculated increments

natural strain - soft soil creep model

Necessary parameters: *a*, *b*, *c*, M, ν

Initial state: p'_o, q_o, p'_{co}. Strains zero.

Test conditions: $d\varepsilon_1/dt$, $d\varepsilon_3/dt$

A series of time steps Δt is defined. For each time step the following steps are performed sequentially:

p_{eq} and p_c are determined from (4.1) resp. (4.4).

Strains are found from the applied rates and the time step Δt.

Incremental secular volume strain is found from (4.9) and the time step Δt.

Incremental secular shear strain is found from (4.11) and the time step Δt.

Incremental stresses are found from (2.8) and (2.9)

Stresses and strains are updated by adding the calculated increments

Such a spreadsheet has been developed and applied in the present study. The original version is due to Fokker (1996). The incremental calculation is sensitive to the size of time step, and a macro has been written to make changes to the time steps easy. Generally, time steps can be gradually increased as the solution progresses.

Note that only single-phase material behaviour is accounted for. Darcy's equation is not considered, and pore pressures are not obtained.

Not only constant rates of strain can be analysed in this way, but actually any sequence of rates of strain. Special cases of interest are alternating rates of vertical strain, relaxation or zero vertical strain rate, and unloading by applying a negative rate of vertical strain.

In chapters 6 and 7, the *a,b,c* isotache model and the natural strain - soft soil creep model will be applied to oedometer and triaxial tests on a soft organic natural Dutch clay. Use is made of the spread sheets described above.

6 Fitting K_o-C.R.S. oedometer tests on natural Oostvaardersplassen clay

6.1 The Constant Rate of Strain K_o oedometer

The tests analysed in this chapter were performed in an oedometer device in which constant rate of vertical strain can be applied, and the lateral stress is measured on the oedometer ring. This apparatus has been developed by GeoDelft and is described by Den Haan, The and Van (2001) in a paper for Geotechniek. A cross section of the apparatus is shown in Figure 1 of the Appendix.

The test is performed in a triaxial cell and the constant rate of strain is applied by the piston in the same way as in a triaxial test. The sample is 63 mm in diameter and initially 20 mm high. It is enclosed in an oedometer ring which has a thin section 0.6 mm thick and 7 mm high. This metal membrane deflects under the lateral load of the sample and this deflection is picked up by strain gauges on its outer surface. The lateral stress follows from calibration.

Drainage is upwards only, and pore pressure is measured at the bottom. Back pressure in the cell ensures sufficient saturation for reliable measurement of the pore pressure. Load cells above and below the sample assembly allow corrections for side friction to be made.

The apparatus yields continuous readings of strain, vertical and horizontal total and effective stresses, side friction loss and pore pressure. The complete stress condition is therefore known, and this makes the results amenable not only to the a,*b,c* isotache model, but also the 2-D version of that model. Various aspects of the K_o Constant Rate of Strain oedometer test will be investigated in this report. In the present section, results of tests on natural Oostvaardersplassen clay will be fitted by the natural strain - soft soil creep model. In other chapters, regard will be given to the relation of $K_{o,nc}$ with other parameters, to loading and unloading in the apparatus, and to relaxation.

In a separate report, "Interpretatie meetdata en parameterbepaling, K_o-C.R.S. proef", CO-710203/22, september 2001, the derivation of the various stresses from the measured quantities is given, together with the parameter determination. That report is meant as an aid for further implementation of the apparatus in routine laboratory practice.

6.2 General properties of the Oostvaardersplassen clay

The test fitted in the section was performed on a sample of natural Oostvaardersplassen clay. The Oostvaardersplassen are a nature reserve immediately north of the city of Almere in the reclaimed polder Zuidelijk Flevoland. The clay is very soft and highly organic, and is from the Almere deposit. The test was performed in the context of a study of sample disturbance which is the subject of GeoDelft report CO-710203/20.

The C.R.S.-K_o test to be fitted is Laval sample number 34 reported in CO-710203/20. Particulars are given in the following table

Table 6.1 Overview of tests and general sample properties

Sampler	Boring - Block/ Sample nr	Depth m - G.L.	Diameter - Height mm	G_s	L.O.I. %	$CaCO_3$ %	ρ_o t/m^3	w_o -	w_{final} -	$w_{o,corr}$ -	v_o -	σ'_{1o} kPa
Laval	34		63 - 20	2.463	14.3	11.1	1.310	1.274	0.982	1.464	4.501	≈18

Three different sampling methods were used at the site: Laval, Begemann and standard tube sampling. The Laval sample exhibits slightly less sample disturbance than the others and appears to be more structured, the normally consolidated region of the stress - strain curve being initially more steep and curving more strongly. The preconsolidation pressure σ'_{1p} is approx. 34 kPa.

6.3 Fits

Fits of the K_o-C.R.S. test on Laval sample nr. 34 were attempted by the 1D *a,b,c* isotache model and 2D natural strain - soft soil creep models, using the spreadsheets discussed in chapter 5. Parameters used in the spreadsheet are given in Table 2. The parameters *a,b,c* were used in the 1D model. The parameters *a*,*b*,*c*, M and ν were used in the 2D model.

Table 6.2 Soil Parameters for natural Oostvaardersplassen clay

a	*a*	*b*	*c*	c/τ_1 day^{-1}	M	ν
0.022	0.0306	0.22	0.0118	1.37E-07	2.06	0.17

Table 6.3 Initial conditions and imposed strain rates -1D model.

σ'_{vp} kPa	σ'_{vo} kPa	$d\varepsilon_1/dt$ sec^{-1}
28.9	3.5	2E-06

Table 6.4 Initial conditions and imposed strain rates - 2D model.

$p'_{c,o}$ kPa	p'_o kPa	q_o kPa	$d\varepsilon_1/dt$ sec^{-1}	$d\varepsilon_2/dt$ sec^{-1}
21	3.5	0	2E-06	0E+00

In Figure 2 the $e_1 - ln\, s'_1$ curves predicted by the 1D and 2D models are shown together with the measured curve. Some observations are:

1. Very good fits to the measured curve are obtained by both models.
2. The model curves bend too sharply near the preconsolidation pressure s'_{1p}.
3. The 2D fit is superior in the overconsolidated region and follows the measured curve quite well. The 1D fit is too straight in the overconsolidated region.
4. The unloading curve is fitted quite well up to an OCR of ≈ 2.0. Thereafter the fits underpredict the swell, the 2D model more than the 1D model.

An initial $\varepsilon_1 = 0.005$ was assumed for both fits, to match the measurements at $s'_1 = 3.5$ kPa. Comments with regard to the observations 2. and 3. are now made.

ad. 2.
The sharp curvatures of the fit near s'_{1p} relative to the measurement expose a shortcoming of creep models. When the soil has been previously loaded and unloaded, the isotaches are distorted during unloading and do not adhere to the patterns as assumed in the model. The model is accurate for states of virginal loading. During unloading and swelling, soil particles undergo a structural change which induces higher rates of creep than would occur at the same stress and strain under virginal conditions. Accurate formulation of the increased rates in the overconsolidated range, i.e. formulation of the distorted isotaches, probably will result in a wider stress range of transition between the two states and result in a less sharp calculated response.

The values taken for the preconsolidation stress need to be considered. The measured value of s'_{1p} may be seen in Figure 2 to be near 34 kPa, and indeed the 1D fit curves sharply at that value of stress. The reference rate of strain in the 1D model is $c/\tau_1 \approx$ 1.37e-7 sec^{-1}. The preconsolidation pressure seen in Figure 2 (34 kPa) is found on an isotache with a rate equal to the applied rate in the test of approx. 2e-6 sec^{-1}. s'_{1p} is sensitive to applied rate, and it is necessary to correct the measured value to obtain the value on the reference isotache. From the geometry of the problem it can be derived that

$$s'_{1pref} = s'_{1p}\left(\frac{c/t_1}{C}\right)^{c/(b-a)} \qquad (6.1)$$

where C is the applied rate. In the present case this entails a 14% reduction, and s'_{1pref} on the reference isotache is 28.9 kPa.

The value of p'_{co} in the 2D fit is 21 kPa and corresponds to the equivalent isotropic stress at s'_{1p} together with the corresponding K_o ratio of approx. 0.34.

ad. 3.

The relationship (4.3) between a and a does not yield the optimal fit. At unchanged a =0.0306, (4.3) gives a=0.0144, but a 50% higher value, a=0.022 has been used. The former value of a grossly underpredicts settlement in the overconsolidated branch. (4.3) is apparently erroneous, although it is much used. Because K_o is not constant in (4.2), there is no simple relationship between both parameters, and both models yield differently shaped predictions. Apparently that of the 2D model is superior.

ad. 4.
The unload branch is discussed in the light of Figures 11 and 12 further on.

Further results for the 2D fit are shown in Figures 3 and 4. Shown are the $e_1 - ln s'_1$, the $e_1 - ln\, p'$, the $K_o - ln s'_1$, and the $s' - t$ relationships. Measurements and fits are shown together.

The $e_1 - ln\, p'$ curve is approximately as well fitted as the 2D fit of the $e_1 - ln s'_1$ curve, but again the fit is rather more sharply curved near the preconsolidation pressure p'_c than the measured curve. K_o is also fitted rather well, as is the general stress path (shown in s´ - t space in Figure 4). However, the increase in fitted K_o near s'_{1p} resp. p'_c is also more acute than was measured. But the decrease of K_o up to s'_{1p} is captured very well. Measured K_o after 35% strain is inaccurate due to a testing deficiency, and is not plotted. The s´ - t curve is also well fitted, although here too the fit is too sharp near s'_{1p}.

The unloading behaviour is captured quite well initially, but increasingly large differences occur after OCR exceeds 2.0. The fitted unloading curves quickly become completely determined by the elasticity parameter ν as the secular rates of strain quickly diminish. Thus $K_o \approx \nu/(1-\nu)$ during unloading. This explains the parallellity of the reloading and unloading $K_o - ln s'_1$ curves in Figure 3.

6.4 The parameter *c* in the K_o-C.R.S. test

One last aspect of the 1D model needs attention. Amongst the parameters of the model is c, which raises the question whether the model can be used to derive this parameter. The answer is that it can not. The virgin part of the curve is essentially an isotache with constant rates of total, direct and secular strain (See chapter 8.1). Knowing the total rate (applied), and the direct rate through a in (3.2), the secular rate is found. This equals, see (3.4), c/τ where τ is the intrinsic time on the measured virgin curve. There is no way of knowing this τ and consequently c cannot be determined independently. The value used here was deduced from fitting triaxial tests on the same material with the 2D model, see chapter 7.

The report Den Haan, E.J. (2001). "Interpretatie meetdata en parameterbepaling, K_o-C.R.S. proef", GeoDelft report nr. CO-710203/22 shows how to determine c from the K_o-C.R.S. test, using either creep stages, variable rates of strain or a relaxation stage.

7 Fitting triaxial tests on natural Oostvaardersplassen clay

A series of triaxial tests was performed as part of the same investigation from which the K_o-C.R.S. tests studied in chapter 6 were taken. Again, only Laval samples are studied in this report. The Oostvaardersplassen clay used for the triaxial tests is from slightly greater depth than the K_o-C.R.S. samples, and is consequently somewhat softer, more organic and higher in water content. The general properties of the triaxial test samples is not given here, but the values of Table 6.1 can be taken as giving indicative values, erring on the stiff side.

The following triaxial tests were performed:
2 UU (unconsolidated undrained) tests
1 CIU (isotropically consolidated, undrained) test at $s'_3 = 25$ kPa
2 CAU (anisotropically consolidated, undrained) tests at $s'_3 = 50$ kPa
2 CAU (anisotropically consolidated, undrained) tests at $s'_3 = 100$ kPa

The undrained shear phase of these tests has been fitted with the 2D model. The soil parameters, initial conditions and imposed rates of undrained shear are shown in Table 7.1. The effective stress paths and the stress - strain paths in shear are shown in Figures 5 and 6.

Table 7.1 Soil parameters, initial conditions and imposed rates, triaxial tests

	UU	CIU25	CAU50	CAU100
a	0.02	0.02	0.015	0.015
b	0.28	0.25	0.28	0.30
c/τ_1 1/day	1.88E-07	1.66E-07	1.92E-07	2.06E-07
M (φ'_{cs})	3 (90°)	2.5 (62°)	2.4 (59°)	2.06 (50°)
m	16	16	16	16
c	0.0162	0.0144	0.0166	0.0178
ν	0.15	0.15	0.15	0.15
$p'_{c,o}$ kPa	11	21	33	72
p'_o kPa	6.2	24	33.5	66.5
q'_o kPa	0	0	25	51.5
$p'_{eq,o}$ kPa	6.2	24	36.7	75.9
$d\varepsilon_1/dt$ 1/sec	1.39E-06	1.39E-06	1.39E-06	1.39E-06
$d\varepsilon_2/dt$ 1/sec	-6.94E-07	-6.94E-07	-6.94E-07	-6.94E-07

The initial stresses and imposed rates correspond to the test conditions. The soil parameters were varied per test to obtain reasonable fits.

The parameter M was chosen to fit the peak strength per test. The corresponding values of φ'_{cs} are shown, and these are very high. The UU test fails on the tension cut-off, and as consolidation pressure increases, M and φ'_{cs} decrease with increasing consolidation pressure (from left to right in the table and graph). These high values of φ'_{cs} are characteristic of soft Dutch clays and are due to the organic material present in the clay. Higher organic content correlates with higher φ'_{cs}.

The most influential parameter in determining the effective stress path in Figure 5 is p'_{co}, which determines the initial rate of creep strain. In all cases it is close to the value of p'_{eqo} and this is due to the strains being defined relative to the beginning of the undrained shear stage. That is, in the figure in chapter 4 showing the principle of the 2D model, strain origin is updated to the beginning of the shear stage, and p'_{co} is updated accordingly. However, small changes in p'_{co} profoundly influence the shape of the effective stress path. For example, increasing p'_{co} by only 2 kPa in the CAU50 test (35 kPa rather than 33 kPa) increases the distance of the stress path to the origin by approx. 6%.

The chosen value of *b* is generally higher than was used for the K_o-C.R.S. test and this reflects the higher water contents of the triaxial samples.

Some observations are made on the attempted fits:

1. Reasonable fits to the measured curve are obtained for all tests.
2. The model t - ε_1 curves bend too sharply near peak strength
3. The model can not simulate the softening of the effective stress paths
4. The UU tests are modelled initially by largely elastic behaviour, resulting in a t - s´ path under a slope of 3:1. The test itself is more complex and only approximately can it be simulated by elastic behaviour. The value of p'_{co} = 11 kPa was used, but this should be closer to 21 kPa to reflect the overconsolidation of the sample. Then, elastic behaviour would be even stronger in the simulation.

An attempt was made to fit the anisotropic consolidation stage of a CAU50 and a CAU100 tests. Both tests were first isotropically consolidated to 25 kPa, and then a rate of vertical strain of 1.39e-6 sec^{-1} was imposed until the required initial deviatoric stress of the undrained shear stage was reached, and the cell pressure was increased in proportion to the deviatoric stress to reach the desired initial cell pressure at the beginning of the shear stage. These paths are shown in Figure 7 together with the fits. The fits were obtained using the measured strains as input and the following parameters were assumed:

Table 7.2 Parameters for fitting anisotropic consolidation stages

	CAU50	CAU100
a	0.028	0.052
b	0.28	0.30
c/τ_1 1/day	1.68E-07	1.50E-07
M	1.9	2.3
m	16	16
c	0.0145	0.0130
ν	0.17	0.17
$p'_{c,o}$ kPa	21	21
p'_o kPa	26.17	24.87
q'_o kPa	3.34	0

The choice of *a* was adjusted to achieve the initial consolidation pressure of 25 kPa using the measured strains in that stage. The value of M was adjusted to fit the maximum measured value of q.

If the simulation is correct, then significant pore pressures are generated during the application of the anisotropic stresses, in both tests. A long consolidation period of more than 3 days was allowed in both tests to dissipate the pore pressures. This phase is not simulated: the simulation is very sensitive to the inevitable oscillations in the measured values which are due to measurement inaccuracy.

In summary, the triaxial tests can be reasonably fitted with the soft soil creep isotache model. It is even likely that the various stages of a test such as isotropic consolidation, anisotropic consolidation and undrained shear, can be modelled with one set of parameters, but sufficient data is lacking to check this. The fits are very sensitive to the values assumed for the initial rates of creep deformation.

Within an embankment or in the vicinity of a structure, it is usually possible to define initial stresses quite well, but the initial amount of *creep* strain and the initial rate of creep are unknown. This is the most vulnerable aspect of the soft soil creep model. This will require constant careful attention when applying the model in practice.

8 1-D Constant Rate of Strain compression

8.1 $K_{o,nc}$ as function of M, n, a, b

In this section, the value of K_o in the normally consolidated state, $K_{o,nc}$, will be derived as a function of M, ν, *a* and *b*.

During a constant rate of strain test,

$$\begin{aligned} \dot{\varepsilon}_1 &= C \\ \dot{\varepsilon}_3 &= 0 \end{aligned} \tag{8.1}$$

Not only the total rate of strain in the vertical direction is constant, but also the direct and secular rates. The basic equations (2.11), (2.12), (4.12), (4.13)

$$\begin{aligned} \dot{\varepsilon}_1^d &= \frac{a}{3}\frac{\dot{p}'}{p}\left(1+2b\frac{\dot{q}}{\dot{p}'}\right) \\ \dot{\varepsilon}_3^d &= \frac{a}{3}\frac{\dot{p}'}{p}\left(1-b\frac{\dot{q}}{\dot{p}'}\right) \\ \dot{\varepsilon}_1^s &= \frac{c}{3t_1}\left(\frac{p'_{eq}}{p'_c}\right)^{\frac{b-a}{c}}\left(1-\frac{h^2-6h}{M^2}\right) \\ \dot{\varepsilon}_3^s &= \frac{c}{3t_1}\left(\frac{p'_{eq}}{p'_c}\right)^{\frac{b-a}{c}}\left(1-\frac{h^2+3h}{M^2}\right) \end{aligned} \tag{8.2}$$

are related by

$$\begin{aligned} \dot{\varepsilon}_1^d + \dot{\varepsilon}_1^s &= C \\ \dot{\varepsilon}_3^d + \dot{\varepsilon}_3^s &= 0 \end{aligned} \tag{8.3}$$

If a constant $K_{o,nc}$ is obtained during constant rate of strain compression then

$$h_{Ko} = \frac{q}{p'} = \frac{\dot{q}}{\dot{p}'} \tag{8.4}$$

Using (8.3), the power in (8.2) can be eliminated to yield

$$\frac{\dot{p}'}{p'} = C\left[\frac{a}{3}\left(1+2b\,h_{Ko}\right) - \frac{a}{3}\left(1-b\,h_{Ko}\right)\frac{\left(M^2-h_{Ko}^2+6h\right)}{\left(M^2-h_{Ko}^2-3h\right)}\right]^{-1} \tag{8.5}$$

The right hand side consists solely of constants and consequently $\dot{p}'/p'$ is constant. Then from (8.2) it follows that $\dot{\varepsilon}_1^d$ and $\dot{\varepsilon}_3^d$ are constant, and from (8.3) also that $\dot{\varepsilon}_1^s$ and $\dot{\varepsilon}_3^s$ are constant. All constituent rates are therefore constant during a constant rate of strain test, in addition to the imposed constant total rate of strain $\dot{\varepsilon}_1 = C$. The stress - strain state will therefore follow an isotache and

$$\dot{\varepsilon}_1 = b\frac{\dot{p}'}{p'} \tag{8.6}$$

and using (8.1) and substituting in (8.5) we find:

$$b = \frac{a}{3}(1+2b\,h_{Ko}) - \frac{a}{3}(1-b\,h_{Ko})\frac{\left(M^2 - h_{Ko}^2 + 6h\right)}{\left(M^2 - h_{Ko}^2 - 3h\right)} \tag{8.7}$$

also to be written as

$$h_{K_o}{}^3 - \frac{b}{a\,b}h_{K_o}{}^2 - (M^2 + 3\frac{b}{a\,b} - \frac{3}{b})h_{K_o} + M^2\frac{b}{a\,b} = 0 \tag{8.8}$$

which in turn can be written as in the Plaxis manual:

$$M = 3\sqrt{\frac{(1-K_0^{NC})^2}{(1+2K_0^{NC})^2} + \frac{(1-K_0^{NC})(1-2n_{ur})(l^*/k^*-1)}{(1+2K_0^{NC})(1-2n_{ur})\,l^*/k^* - (1-K_0^{NC})(1+n_{ur})}} \tag{8.9}$$

if b is replaced by λ^* and a by κ^*. The same equation applies to the inviscid model, and neither rate of strain nor coefficient of rate of secular compression (c) influence η_{Ko}. This is a remarkable finding, which illustrates that the inviscid and viscid versions of the Camclay model are very closely linked.

Note that in the original publication of the Modified Camclay model (Roscoe and Burland, 1968), no elastic shear occurred under the yield surface. As a result, a somewhat more simple equation was obtained in which ν does not figure:

$$h_{K_o}{}^2 + 3(1-\frac{a}{b})h_{K_o} - M^2 = 0 \tag{8.10}$$

Equation (8.8) is quite complex. It is shown as K_o vs. M in Figure 8 and Figure 9 for various $b/\kappa b$ resp. b/κ (where κ is identical to a) and ν values. The M-scale is taken to values in excess of 2 ($\varphi' \approx 50°$) to cope with the high measured values of φ' in organic clays.

For a given value of b/κ (or b/a), there is a range of curves for different ν values, the width of the range decreasing as b/κ (b/a) increases. Finally, at high b/κ (b/a), ν no longer influences the K_o vs. M relationship. For low values of ν as will usually be applied in the present model, K_o is only weakly dependent on ν.

When elastic deformations are excluded by putting $\kappa = a = 0$, both the present solution for h_{Ko} (8.8) and the Roscoe and Burland equation (8.10), simplify to

$$h_{Ko}{}^2 + 3h_{Ko} - M^2 = 0 \tag{8.11}$$

or

$$K_o = \frac{9}{2\sqrt{9+4M^2}} - \frac{1}{2} \tag{8.12}$$

This is the *upper*bound solution for Burland & Roscoe's case: they considered values of a/b up to 0.6 which places the line lower, and quite close to Jáky given by

$$K_o = 1 - \sin\varphi' = \frac{6-2M}{6+M} \tag{8.13}$$

8.2 $K_{o,nc}$ equations from other sources

Many equations have been given in the past relating $K_{o,nc}$ to parameters such as M or φ', I_p, κ/λ (a /b), ν etc. Increasing φ' results in decreasing $K_{o,nc}$ in all such equations. The organic clays of the Netherlands have much higher φ' than is usual in inorganic soft clays, and $K_{o,nc}$ appears to be lower than in inorganic clays. Possibly then, extrapolation of existing relationships to higher φ' would fit the Dutch organic clay. This will be investigated here.

Cherubini & Giasi (1995), Lareal et al. (1995) and Szepesházi (1995) give useful overviews of the many $K_{o,nc}$ equations in the literature. Of those using φ', the following are investigated:

Jáky (1944): $(1 + 2/3 \sin \varphi')(1 - \sin \varphi')/(1 + \sin \varphi') = (6+3M)*(6-2M)/(6+M)/6+4M)$
$\approx (1 - \sin \varphi')$ for sands
$\approx (0.95 - \sin \varphi')$ for clays

Wenkow (1979): $\tan(45° - \varphi'/2)$

Vierzbiczky (mentioned by Rymsza 1979): $\tan^2(45° - \varphi'/3)$

Fraser: $0.9(1 - \sin \varphi')$

Yamaguchi (1972): $(1 - 0.404 \tan \varphi')/(1 + \sin \varphi')$

Simpson (1992): sands and clays: $(\sqrt{2} - \sin \varphi')/(\sqrt{2} + \sin \varphi')$

Brooker and Ireland (1965): $\approx (0.95 - \sin \varphi')$ for clays

Mayne and Kuhlhawy (1982): $1 - 1.003 \sin \varphi'$

Kutter & Sathialingam (1992) : $4.5/\sqrt{(9+4M^2)} - 0.5$

The latter solution by Kutter & Sathialingam is given by them as an approximate solution for K_o consolidation of their model which is completely similar to the present 2D model (differing only in using linear rather than logarithmic strain) and the Plaxis soft soil creep model. It is found by assuming zero elastic strains on the K_o path, and this approximation therefore equals (8.12). However, it will be shown in section 8.4 that this solution is more exactly the value to which K_o gradually increases if creep at constant vertical effective stress occurs.

The various equations are shown in Figure 10. The Jáky solution is an approximate lower bound to all equations, while Roscoe & Burlands κ/b=0 case is an approximate upper limit. Plotted in the figure are data from the 2 Dutch clays to date for which the M and $K_{o,nc}$ are both known. These are both light clays with a γ_{tot} of approx. 1.25 t/m^3. The Bergambacht clay, described in Tigchelaar (2001) fails consistently on the tension cut-off with $s'_3 = 0$ so M=3.

The Oostvaardersplassen clay falls in the extension to high M of the existing equations. Wenkow's equation especially is very close and also comes from near Jáky's equation at lower (more usual) values
of M, which is probably realistic. The Bergambacht clay lies well outside all equations. Jáky grossly underpredicts both clays.

As the K_o-C.R.S. oedometer gradually finds more application, the M - $K_{o,nc}$ correlation will be further refined for Dutch organic clays.

8.3 Development of strain and $K_{o,nc}$ during ageing

The development of K_o during ageing has been intensely discussed after Schmertmann (1983) asked "a simple question about consolidation". At that time, no serious thought had yet been given to whether K_o increases, decreases or remains essentially constant during ageing. Schmertmann had canvassed opinions among a number of experienced geotechnicians and found that the majority of them favoured an *in*crease of K_o during ageing. After much research and discussion, consensus has grown that soft clays indeed increase their K_o during ageing, but the rate of increase is very slow. The present model predicts a development of K_o with time which is usually an increase, but sometimes a decrease.

The imposed conditions during ageing are

$$\delta\sigma_1' = 0 \tag{8.14}$$

from which (2.4) yields

$$\frac{\delta q}{\delta p'} = -\frac{3}{2} \tag{8.15}$$

and

$$\delta\varepsilon_3 = \delta\varepsilon_3^d + \delta\varepsilon_3^s = 0 \tag{8.16}$$

From (2.8) and (2.9), the ratio of $\delta q / \delta p'$ follows as

$$\frac{\delta q}{\delta p'} = \frac{1}{b}\frac{\delta\varepsilon_1^d - \delta\varepsilon_3^d}{\delta\varepsilon_v^d} \tag{8.17}$$

giving the difference of the principal direct strain rates as

$$\delta\varepsilon_1^d - \delta\varepsilon_3^d = -\frac{3}{2} b\, \delta\varepsilon_v^d \tag{8.18}$$

The difference of the principal secular strain rates follows from (4.10) as

$$\delta\varepsilon_1^s - \delta\varepsilon_3^s = \frac{3}{2}\delta\varepsilon_s^s = \frac{3}{2}\frac{2h}{M^2 - h^2}\delta\varepsilon_v^s \tag{8.19}$$

Adding these equations, the sum of the minor principal strain rates on the LHS becomes zero leaving the LHS to equal the major principal strain rate. The rate of secular volume change is replaced by the difference of the total and direct rates of volume change, and the total rate of volume change is replaced in turn by the total major principal rate of strain to which it is equal. This finally results in

$$\delta\varepsilon_1 = \delta\varepsilon_v^d \frac{\left(-\frac{3}{2}b - \frac{3}{2}\frac{2h}{M^2 - h^2}\right)}{\left(1 - \frac{3}{2}\frac{2h}{M^2 - h^2}\right)} = \frac{a\,\delta p'}{p'}\frac{\left(-\frac{3b}{2}h^2 + 3h + \frac{3\,b\,M^2}{2}\right)}{\left(h^2 + 3h - M^2\right)} \tag{8.20}$$

This equation can be integrated in time starting from the conditions at the beginning of the ageing. The spreadsheet described earlier can be adapted to determine an increment of vertical strain given an increment of p´. The time increment associated with this stress change is found from

$$\Delta t = \frac{\Delta e_v - \Delta e_v^d}{\dot{\varepsilon}_v^s} = \frac{\Delta e_1 - \Delta e_v^d}{\dot{\varepsilon}_v^s} = \frac{\dfrac{a\,\Delta p'}{p'}\dfrac{\left(-\dfrac{3b}{2}h^2 + 3h + \dfrac{3\,b\,M^2}{2}\right)}{\left(h^2 + 3h - M^2\right)} - \dfrac{a\,\Delta p'}{p'}}{\dfrac{c}{t_1}\left(\dfrac{p'_{eq}}{p'_c}\right)^{\frac{b-a}{c}}\left(1-\dfrac{h^2}{M^2}\right)} \tag{8.21}$$

Deformation continues indefinitely, at a slope c on a e_1 vs. -log($\dot{\varepsilon}_1$) plot. Such a relationship between e_1 and $\dot{\varepsilon}_1$ at constant s_1 may be termed an "isobar". Thus, all ageing occurs on isobars at constant slope c. The stress ratio η during ageing approaches an asymptotic final value as given in 8.4.

An explicit equation for the development of K_o during ageing as a function of time has not been derived, but in 8.4 calculations are presented which demonstrate it.

8.4 Final value of $K_{o,nc}$ during creep

Ultimately during ageing under constant s'_1, stress will reach a final value. Consequently, elastic deformation will cease. Only the secular deformation will persist. Therefore:

$$\left.\begin{array}{l}\dot{\varepsilon}_1^d = \dot{\varepsilon}_3^d = 0 \\ \dot{\varepsilon}_3 = 0\end{array}\right\} \dot{\varepsilon}_3^s = 0 \tag{8.22}$$

The proportionality factor of $\dot{\varepsilon}_3^s$ in (4.13) must therefore also equal zero. Writing h_∞ for the asymptotic value of the stress ratio,

$$h_\infty^2 + 3h_\infty - M^2 = 0 \tag{8.23}$$

This is identical to (8.11) for the case of zero elastic deformation. It is also identical to the solution of the Roscoe and Burland model for a/b=0 that is zero elastic deformation.
It will be clear that if there is no elastic deformation, the value of η during compression under increasing vertical stress (e.g. Constant Rate of Strain) will equal the final value, and K_o will not change during ageing. Otherwise, equation (8.8) will hold during compression under increasing vertical stress, and equation (8.23) will give the final value of η and K_o. It will depend on the relative magnitude of η_{Ko} and η_∞ whether K_o will increase or decrease during ageing to the final value. In Figures 8, 9 and 10 the asymptotic value of K_o is the Roscoe and Burland solution for a/b =0, and it can be seen that the present model will give both increasing and decreasing K_o during ageing depending on the values of a/b and ν. Low values of ν, which are probably realistic, will tend to give an increase of K_o.

Kutter and Sathialingam (1992) also derived equation (8.23), but viewed it as an approximate solution along the K_o consolidation line. However, that condition is covered more correctly by (8.8). The latter equation was not derived by them.

Figures 11 and 12 shows the development of K_o with time for an assumed case. The K_o-C.R.S. test performed on Laval sample nr. 34 of Oostvaardersplassen clay which was fitted in chapter 6, see Figures 2, 3 and 4, will be used. The fitted soil parameters, the initial condition and the rate of strain are taken as in chapter 6. The Constant Rate of Strain loading, which was up to s'_1 = 490 kPa in the

test, is now interrupted at various values of s_1' to allow ageing at constant s_1'. Ageing is calculated at s_1' = 10, 30, 100, 200 and 490 kPa. Further, the effect of unloading on ageing is studied by unloading from s_1' = 200 kPa from s_1' = 100 kPa and again from 490 kPa to 100 kPa, and calculating the ensuing ageing.

In Figure 11 the C.R.S. loading up to s_1' = 490 kPa yields the same values of K_o as plotted in Figure 3. K_o starts from high values at the beginning of the test, where the OverConsolidationRatio is high. K_o falls as the preconsolidation pressure s_{1p}' is approached at 34 kPa. Again the steep rise is found in the vicinity of the preconsolidation pressure, as was also found in Figure 3. K_o increases gradually after s_{1p}' to the final virgin value (equation (8.8)) of K_o is 0.3711.

Ageing at s_1' = 10 kPa gives a very gradual decrease of K_o to the asymptotic final value of 0.3830 (equation (8.23)). This is seen more clearly on Figure 12 where the time axis is extended. Ageing at s_1' = 30, 100, 200 and 490 kPa produces in each case an increase of K_o to the asymptotic value. It may be concluded that ageing will always bring K_o to the asymptotic value, and that both increases and decreases of K_o may be associated with this, depending on the initial value of K_o at the beginning of ageing. Note however that the time scale in Figure 12 (10^{14} days) exceeds the postulated age of the universe ($2\,10^{12}$ days)!

In Figure 12, Constant Rate of Strain unloading from 200 kPa resp. 490 kPa is shown, together with subsequent ageing at 100 kPa. Again ageing brings K_o gradually to the asymptotic value. However, the period of time associated with full ageing of K_o is strongly dependent on the OverConsolidationRatio. The ageing at 10 kPa, and the ageings after unloading from 200 resp. 490 kPa to 100 kPa have OCR values of resp. 3.4, 2 and 4.9, and full ageing occurs after approx. $1.5\,10^9$, $3\,10^5$, and $3\,10^{12}$ days. Effectively, K_o remains constant during long periods.

8.5 Relaxation

Viscous materials exhibit relaxation (stress reduction) when strains are restrained from occurring. In oedometer tests with full piston control such as is used for Constant Rate of Strain testing it is a matter of preventing piston deformation and measuring the change of stress necessary to achieve this. A number of relaxation tests have been performed with the GeoDelft K_o-C.R.S. apparatus and these will be analyzed here.

1-D (oedometric) relaxation will be considered. It will be studied in both the 1-D *a,b,c* model and its 2-D generalization. Relaxation as a stage in a C.R.S. oedometer test can be used to determine the *c* parameter which describes viscous behaviour in the 1-D *a,b,c* isotache model. See Figure 13. In the generalized 2-D model, relaxation gives different equations than the 1-D model, and involves the shear strength parameter M and Poisson's ratio.

8.5.1 Relaxation in the 1-D *a,b,c* model

The state at start of relaxation is designated by $_R$. Strains e^d and e^s counter each other during relaxation:

$$\dot{\varepsilon}_1 = 0; \qquad \dot{\varepsilon}_1^d = -\dot{\varepsilon}_1^s \tag{8.24}$$

Direct strain rate is given by

$$\dot{\varepsilon}_1^d = \frac{a}{\sigma'_1}\dot{\sigma}'_1 \tag{8.25}$$

and secular strain rate by (see (3.6))

$$\dot{\varepsilon}_1^s = \dot{\varepsilon}_{1R}^s \left(\frac{\sigma'_1}{\sigma'_{1R}}\right)^{\frac{b}{c}} \exp\left(\frac{-(e_1 - e_{1R})}{c}\right) = \dot{\varepsilon}_{1R}^s \left(\frac{\sigma'_1}{\sigma'_{1R}}\right)^{\frac{b}{c}} \tag{8.26}$$

in which has been applied that $e_1 - e_{1R} = 0$, so that

$$\frac{a\dot{\sigma}'_1}{\sigma'_1} = -\dot{\varepsilon}_{1R}^s \left(\frac{\sigma'_1}{\sigma'_{1R}}\right)^{\frac{b}{c}} \tag{8.27}$$

Separating variables and integrating:

$$\int_{\sigma'_{1R}}^{\sigma'_1} \frac{\dot{\sigma}'_1}{\sigma'_1}\left(\frac{\sigma'_1}{\sigma'_{1R}}\right)^{-\frac{b}{c}} = -\int_0^t \frac{\dot{\varepsilon}_{1R}^s}{a} \tag{8.28}$$

$$\frac{-c}{b}\left(\frac{\sigma'_1}{\sigma'_{1R}}\right)^{-\frac{b}{c}} \Bigg|_{\sigma'_{1R}}^{\sigma'_1} = -\frac{\dot{\varepsilon}_{1R}^s}{a}t \tag{8.29}$$

$$\left(\frac{\sigma'_1}{\sigma'_{1R}}\right)^{\frac{-b}{c}} - 1 = \frac{b}{ac}\dot{\varepsilon}_{1R}^s t \tag{8.30}$$

$$\sigma'_1 = \sigma'_{1R}\left[1 + \frac{b}{ac}\dot{\varepsilon}_o^s t\right]^{\frac{-c}{b}} = \sigma'_{1R}\left[1 - \frac{b}{c}\frac{\dot{\sigma}'_{1R}}{\sigma'_{1R}}t\right]^{\frac{-c}{b}} \tag{8.31}$$

The secular strains are countered by the direct strains, and so the creep isotaches in ln σ'_1 - e_1^s space are intersected at the slope -a. However, the deformation does not actually occur, and it is quite probable that creep rates on isotaches are sensitive to true deformations. During loading, strains can be separated into direct and secular components while at the same time maintaining the dependency of secular rate on true deformation. During relaxation, this is seen not to be the case. Therefore, it may be preferable to intersect the creep isotaches horizontally. Then , writing the first equation of (8.26) in terms of secular strains, and applying $e_1^s - e_{1R}^s = 0$:

$$\dot{\varepsilon}_1^s = \dot{\varepsilon}_{1R}^s \left(\frac{\sigma'_1}{\sigma'_{1R}}\right)^{\frac{b-a}{c}} \exp\left(\frac{-(e_1^s - e_{1R}^s)}{c}\right) = \dot{\varepsilon}_{1R}^s \left(\frac{\sigma'_1}{\sigma'_{1R}}\right)^{\frac{b-a}{c}} \tag{8.32}$$

It may be shown that (8.31) then mutates to

$$\sigma'_1 = \sigma'_{1R}\left[1 + \frac{b-a}{ac}\dot{\varepsilon}_o^s t\right]^{\frac{-c}{b-a}} = \sigma'_{1R}\left[1 - \frac{b-a}{c}\frac{\dot{\sigma}'_{1R}}{\sigma'_{1R}}t\right]^{\frac{-c}{b-a}} \tag{8.33}$$

This equation is preferred. It can be used to determine c from a relaxation stage in an oedometer test, knowing a, b, and the initial value σ'_{1R} and rate of change $\dot{\sigma}'_{1R}$ of the vertical effective stress. This has been done for the results of a K_o-C.R.S. test (nr. 17C+) on a peat from Barendrecht, see Den Haan et al. (2001). Figure 14 shows the results. In the inset of the figure, the stress - strain relationship is shown together with that of a standard incremental loading (24 h per stage) oedometer test on a nearby sample (nr. 17D). The proximity of both curves demonstrates their similarity when the applied strain rate in the C.R.S. test is $2\ 10^{-6}$ 1/s. (The vertical scale in the inset is shown as ε^H which designates natural strain). The two relaxation curves from stresses of resp. 140 and 180 kPa have been fitted by a single set of values of a, b and c. Data on/from the tests are given in the tables below.

Table 8.1 Soil Parameters for peat from Barendrechtseweg, sample nr. 17C+

depth m-G.L.	ρ_{tot} kN/m^3	a	b	c	σ'_{1p} kPa	$K_{o,nc}$
2.40-2.60	1.039	0.0403	0.287	0.0240	60	0.35

Table 8.2 Strain rates immediately before and after the beginning of relaxation, peat sample nr. 17C+, Barendrechtseweg

σ'_{1R} kPa		$\frac{d\sigma'_1}{dt}$ kPa/s	$\frac{d\varepsilon_1^d}{dt}$ 1/s (a=0.0403)	$\frac{d\varepsilon_1^s}{dt}$ 1/s	$\frac{d\varepsilon_1}{dt}$ 1/s
32 (after unloading)	before	-2.00E-03	-2.52E-06	5.89E-07	-1.93E-06
	after	3.20E-03	4.03E-06	-4.03E-06	0
141.9	before	1.20E-03	3.41E-07	1.62E-06	1.96E-06
	after	-4.46E-03	-1.27E-06	1.27E-06	0
181.3	before	1.76E-03	3.91E-07	1.56E-06	1.95E-06
	after	-7.57E-03	-1.68E-06	1.68E-06	0

8.5.2 Relaxation after unloading

In Figure 14 it is shown how the 1-D *a,b,c* isotache model is successfully applied to the relaxation phases starting from $\sigma'_{1R} = 140$ resp. 180 kPa. However, a relaxation phase was also applied in the considered test (nr. 17C+) at the end of the unloading phase from approx. $\sigma'_1 = 90$ kPa to 32 kPa. Table 8.2 lists rates of stress change and the various strain rates immediately prior to and immediately after the beginning of relaxation for the three relaxation stages. The rate of stress change $\dot{\sigma}'_1$ is determined directly from the measured data, and $\dot{\varepsilon}_1^d$ is found from $\dot{\sigma}'_1$ through (8.25) by assuming a=0.0403. The rate of secular strain $\dot{\varepsilon}_1^s$ then follows from the difference of the applied total rate and the calculated direct rate.

The values of $\dot{\varepsilon}_1^s$ in Table 8.2 before and after the beginning of relaxation are reasonably similar for the higher stages (140 resp. 180 kPa), and the small differences can be attributed to measurement error, or a not being the same in loading and unloading.

However, after unloading to 32 kPa, the rate of secular strain changes abruptly from approx. 0.6 10^{-6} (compressive) to approx. -4 10^{-6} 1/s. Isotache models assume that secular strain rates depend uniquely and smoothly on stress and strain, and do not allow for such jumps. Further, they also do not account for negative rates of secular strain.

The relaxation equation (8.33) does not account for negative rates of secular strain. It does predict *increasing* stress with time if a positive initial rate of stress change is input into it, but the stress increases very quickly with time and becomes infinite when the argument of the power (the expression between straight brackets in (8.33)) becomes zero. In the present case this is after approx. 1000 sec. Again however, the equation is not valid in this case.

It is clear that the behaviour exhibited during relaxation after unloading:
* increasing stress,
* positive direct strain rate,
* negative secular strain rate
* a jump in secular strain rate.

cannot be modelled by isotache models. This behaviour was found in other tests as well, and apparently represents true soil behaviour. There are other aspects of unloading and reloading presently not accounted for in any available models which need consideration. This will be addressed in chapter 8.6.

8.5.3 1-D Relaxation in the 2-D model

Having the 2-D model available makes it possible to look at the complete stress state during 1-D relaxation. During 1-dimensional relaxation, all deformation ceases. Then

$$d\varepsilon_1 = d\varepsilon_2 = d\varepsilon_p = d\varepsilon_q = 0 \tag{8.34}$$

$$d\varepsilon_1^e = -d\varepsilon_1^p \; ; \qquad d\varepsilon_2^e = -d\varepsilon_2^p \; ; \qquad d\varepsilon_p^e = -d\varepsilon_p^p \; ; \qquad d\varepsilon_q^e = -d\varepsilon_q^p \tag{8.35}$$

From the third of these latter relationships it follows:

$$\frac{a}{p}\frac{dp}{dt} = -d\varepsilon_c \left(\frac{p_{eq}}{p_c} \right)^m (1 - \frac{q^2}{M^2 p^2}) \tag{8.36}$$

and with $d\varepsilon_2 = 0$

$$\frac{a}{p}\frac{dp}{dt} = \frac{a}{p}\frac{dp}{dt}(1 - b\,\frac{dq}{dp}) \frac{(1 - \frac{q^2}{M^2 p^2})}{(1 - \frac{q^2}{M^2 p^2} - \frac{3q}{M^2 p})} \tag{8.37}$$

$$1 - b\,\frac{dq}{dp} = 1 - \frac{\frac{3q}{M^2 p}}{1 - \frac{q^2}{M^2 p^2}} \tag{8.38}$$

$$\frac{\delta q}{\delta p} = \frac{1}{b} \frac{\frac{3q}{p}}{M^2 - \frac{q^2}{p^2}} \tag{8.39}$$

This equation can be tackled incrementally to give the development of the stress path during relaxation. Only β (i.e., ν) and M appear as parameters, whereas in the 1-D analysis the compressibility parameters *a,b,c* appear.
Figure 15 shows fits to the relaxation phases of the test on peat sample 17C+ from Barendrechtseweg in the p'-q plane. The fits are quite satisfactory. M=2.1, ν=0.17 were chosen for the second and third phases, and M=1, ν=0.17 for the first phase. Note that the *in*crease of q and p' in the first phase is modelled faithfully! The chosen parameters are quite close to values used for the Oostvaardersplassen clay treated in earlier chapters, but this is coincidence. No triaxial tests are available on the peat to test the validity of the derived values of M and ν.

Equation (8.39) may well provide a means to derive strength parameters from the K_o-C.R.S. test!

8.6 Deficiencies of isotache models

In sub-chapter 8.5.1 it was shown that isotache models do not capture the behaviour of relaxation following unloading very well. Further deficiencies exist for other cases.

Distortion of isotaches by unloading
During unloading, isotaches become distorted due to the damage occurring to the soil fabric by the release of stress and the swelling. Secular rates become higher than during virgin loading at the same stress and strain. The shape of secular isotaches during reloading has been discussed by Den Haan and Sellmeijer (2000), who found that hyperbolae in log(stress)-strain space fit the distorted isotaches well in this region. It could be hoped that the same relationship was found for creep at constant stress in the reloading range, but this does not seem to be the case.

Negative rate of secular strain during unloading
Negative secular strain rates occur not only during relaxation following unloading, but also during unloading when the stress reduction exceeds a certain relative magnitude. Swelling then has both a direct component and a secular component, both directed upward. The negative creep is probably associated with the time effect of the structural change brought about by the unloading. Once soil particles start rearranging to accommodate the lower stress, it is likely that it will continue for some time when the stress is arrested. This effect is likely to be greater for a larger unloading, and therefore it may be proportional in some way to the direct component of swell. The overall stress remains compressive however, and after some time the direction of deformation will switch from upwards to downwards again. It is likely that the return to positive secular rates occurs more quickly for smaller unloading.

This effect is rather important. The preloading technique is still one of the most effective ways to reduce settlement of embankments and fills, and predictions of this case require that secular swell and

the ensuing return to secular compression are accounted for. Swelling of the bottom of excavations is another case where this occurs.

Illustration of deficiencies of isotache models.
In the following figure a number of effects is illustrated. The virgin isotaches are straight and equidistant, but the reload isotaches (as measured in incremental loading oedometer tests e.g.) are distorted, and the same secular strain rate occurs at lower stress or larger strain than would occur in virginal circumstances. The regions of virginal and reload isotaches are separated by a horizontal line at a strain which is related to the maximum strain incurred during previous loading.

From the state of stress - strain - strain rate at A, various stress - strain paths are illustrated. Creep may occur at constant stress along AB and the current *a,b,c* model describes this well. Unloading may occur as shown along AD, with both direct swell and secular swell determining the unloading stress-strain path. Creep at constant stress following unloading will result in secular swell, probably more at lower stress. The secular swell will reach a maximum after which secular compression will reappear, probably more at higher stress. If unloading is very limited, the secular swell may be too small to notice.

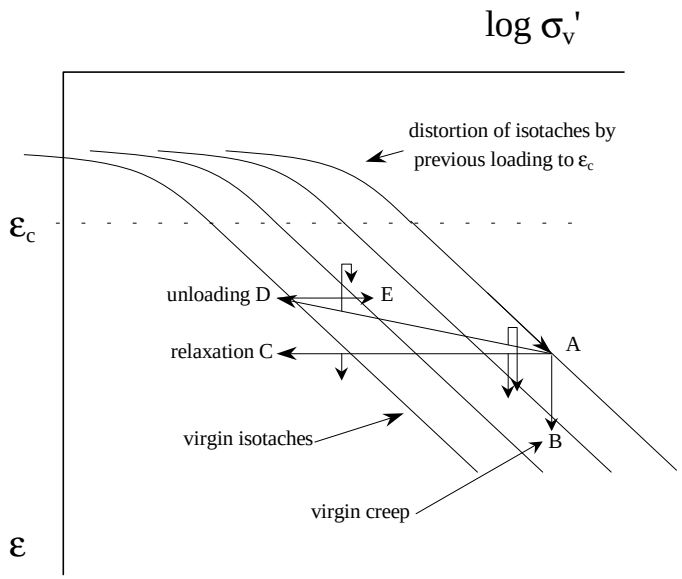

Relaxation after state A will produce a stress - strain path to the left along AC. Soil structure should not change during relaxation, and it may be expected that creep at constant stress following relaxation will produce *compressive* strains, i.e. *positive* secular strains. Tests will be performed in the near future in the GeoDelft K_o-C.R.S. apparatus to verify these postulations.

By formulating a law for the distortion of isotaches due to swelling and accounting for secondary swell, many of the described and postulated aspects of unloading/reloading/relaxation behaviour may be covered. Reloading following unloading and creep following unloading would hopefully adhere to the same model if the secondary swell at the beginning of creep following unloading is accounted for. Relaxation following unloading might also adhere to the same law, making use of the secondary swell to yield *in*creasing stress. But the jump in secular strain rate seen in test 17C+ would not be modelled, and this requires additional modelling.

Bricks on Ice

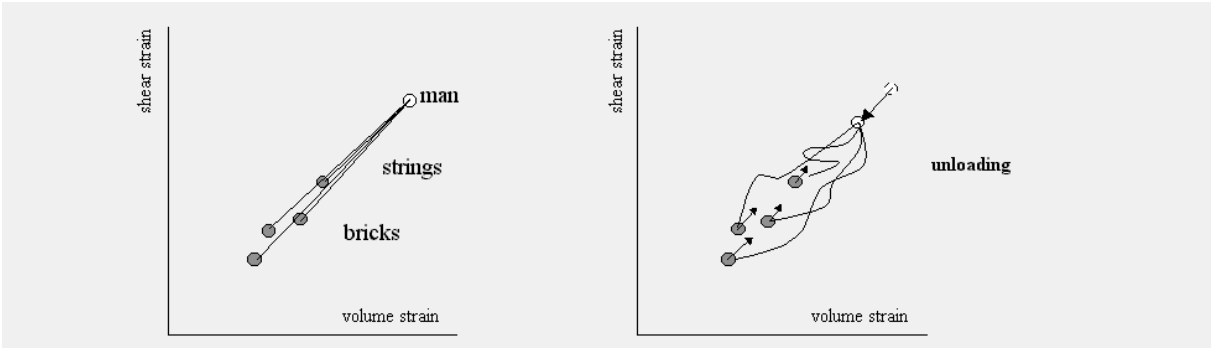

Simpsons' Brick model may well be easily adapted to account for creep. In that model a man pulls a number of bricks each having a string of different length. The movement of the man models total strain, with the coordinates of shear strain and volume strain. The combined movement of the bricks models plastic strains and the difference is the elastic strains. Stresses are proportional to the elastic strains. Prolonged movement in one direction maximizes plasticity and minimizes stiffness. Reversal of movement produces slack strings, zero plasticity and maximum stiffness in the first instance, but gradually plasticity is reasserted as the bricks start moving again one after the other. A flanking movement lets the bricks on short strings follow immediately but the bricks on longer strings first continue in the old direction, and plasticity is first reduced but then slowly redevelops.

Effects of recent stress history (or rather, recent ***strain*** history) are simply and effectively accounted for by the model. By giving each brick a motion of its own which continues even when the strings are slack, viscous behaviour can be introduced. Relaxation is modelliing by letting the man stop. The bricks then continue to approach the man, diminishing the distance to the man, and reducing the elastic strain and the stress.

Creep is modelled by keeping the distance between the bricks and the man constant.

The figure on the right above illustrates unloading. The motion is reversed, but the bricks first continue to move in the former direction. The distance between man and brick is diminished more quickly than in the inviscid case, and stresses reduce likewise. Limited unloading will affect the bricks on the shortest strings: they only will reverse their motion. These then obtain a creep motion in the reversed direction. The bricks on longer strings will keep their original motion and these will take over the weighted, total movement of the bricks when the motion of the bricks on shorter strings dies out. Then, the man will have to reverse his direction to keep the same distance to the bricks.
A larger unloading will affect more bricks and the creep motion in the swelling direction will be enhanced.

When the man has passed a number of bricks during unloading and then stops (relaxation after unloading) then some bricks will be moving in the swelling direction. Subsequent relaxation (man stands still) will result in increasing stress.

Dynamic Bricks
One can wonder what possibilities lie in giving the bricks a mass and damping.

9 Summary and Conclusions

This report has investigated various aspects of the 1-D *a,b,c* isotache model and its generalization to 2-D, only under drained, axially symmetric conditions. Both models are described and equations are given for the relation between stress, strain and strain rate. These can be applied to solve for any arbitrary strain path, and spreadsheets have been developed to facilitate this.

The models are applied to results of Constant Rate of Strain K_o oedometer tests and various triaxial tests (UU, CIU and CAU) on a soft organic clay (natural Oostvaardersplassen clay), and generally very reasonable fits have been obtained. ε_1 - σ'_v, s' - t, K_o - σ'_v relationships were all satisfactorily fitted.

A large part of the report investigates the various values which K_o can take on during 1-D consolidation in the 2-D model. It is found that monotonic loading at any (sequence of) strain rate(s) leads to a normally consolidated value $K_{o,nc}$ which is equal to $K_{o,nc}$ for the inviscid model (e.g. the Plaxis soft soil model without creep). Creep ageing at constant stress results in another value $K_{o,\infty}$ which can be either higher or lower than $K_{o,nc}$. Generally it is slightly higher and this is supported by the majority of the literature on this subject. For high values of the critical state stress ratio M and high values of Poisson's ratio ν it can be lower, and some evidence is provided showing this may be the case for Dutch organic clay. After unloading to an overconsolidated state, K_o again tends towards the same value of $K_{o,\infty}$ but the time scale is greatly extended by even a little overconsolidation, and effectively, K_o remains constant according to this model for substantially overconsolidated clays.

Relaxation in the Constant Rate of Strain K_o oedometer is solved for the 1-D and 2-D models. The 1-D solution provides a useful means of determining the creep parameter *c* from Constant Rate of Strain oedometer tests. The solution for 2-D reveals a relationship between the stress path, ν and M, and this may provide a means of finding M from the test.

Strain fixation ("relaxation") after unloading in the Constant Rate of Strain K_o oedometer does not lead to stress reduction, but rather to stress increase. This behaviour is consistent, and cannot be modelled by the models studied. Other deficiencies of the isotache model are discussed. Essentially soft soil exhibits secular *swell* after unloading, and no models are presently available to model this. It is shown how Simpson's Brick model may possibly be adapted to cope with this behaviour.

Notwithstanding these deficiencies, this study has shown that the creep isotache model is well suited to modelling soft organic clay. In a further study, the application to embankments could be studied.

10 References

Keverling Buisman A.S. (1936). Results of long duration settlement tests. Proc. 1st ICSMFE, Cambridge, Mass. No. F-7:103-106.

Roscoe, K.H. & Burland, J.B. (1968). On the generalized stress-strain behaviour of 'wet' clay. Conference papers, Engineering Plasticity. Ed. J. Heyman & F.A. Leckie. Cambridge at the University Press, pp. 535-609.

J.H. Schmertmann (1983). A simple question about consolidation. Jnl Geot. Eng. Div. A.S.C.E. 109:1

Kutter, B.L. & Sathialingam, N. (1992). Elastic-viscoplastic modelling of the rate-dependent behaviour of clays. Géotechnique 42(3), 427-442.

Den Haan, E.J. (1992). "The formulation of virgin compression of soils." *Géotechnique*, 42(3), 465-483.

B. Simpson (1992). Retaining structures: displacement and design. Rankine Lecture, Géotechnique, 4:541-576.

Den Haan, E.J. (1994). Vertical compression of soils (Doctoral Thesis). Delft University Press, 96pp

Cherubini, C. & Giasi, C.I. (1995). The reliability of expressions for K_o evaluation. Proc. 11th ECSMFE, Copenhagen, Vol. 1, 49-54

Lareal, P., Boulebnane, A., Garnier, J. & Cottineau, L.M. (1995). Experimental investigation of the coefficient K_o. Proc. 11th ECSMFE, Copenhagen, Vol. 3, 143-148

Szepesházi, R. (1995). Some characteristics of the K_o condition. Proc. 11th ECSMFE, Copenhagen, Vol. 6, 197-202

Den Haan, E.J. (1996). A compression model for non-brittle soft clays and peat. Géotechnique, 1:1-16

Fokker, P. (1996). 3D kruip in Ei-model. GeoDelft report nr. SE-59076, may.

Plaxis Version 7 (1998). Manuals -Part 3 Material Model Manual - Chapter 5 Soft Soil Creep Model. A.A. Balkema Rotterdam.

Den Haan, E.J. & Sellmeijer, J.B. (2000). Calculation of soft ground settlement with an isotache model. Geot. Spec. Publication Nr. 112, A.S.C.E., p. 83-104.

Den Haan, E.J. (2001). Consef01.exe, Consef Intro & Exercises.doc, Param Strings.xls (2001). http://www.geodelft.nl/ - research and development - research specialists - dr.ir. E.J. den Haan -. (Executable, description and exercises regarding program Consef)

Den Haan, E.J. (2001). "Sample disturbance of a soft organic Dutch clay ", GeoDelft report nr. CO-710203/20, may.

J. Tigchelaar (2001) Gedrag van organische klei, Bergambacht site. GeoDelft report CO-396180/xx, augustus.

Den Haan, E.J. (2001). "Interpretatie meetdata en parameterbepaling, K_o-C.R.S. proef", GeoDelft report nr. CO-710203/22, september.

Den Haan, E.J., The, B.H.P.A.M. & Van, M.A. (2001). De K_o-C.R.S. samendrukkingsproef. Geotechniek, okt. 55-63.

APPENDICES

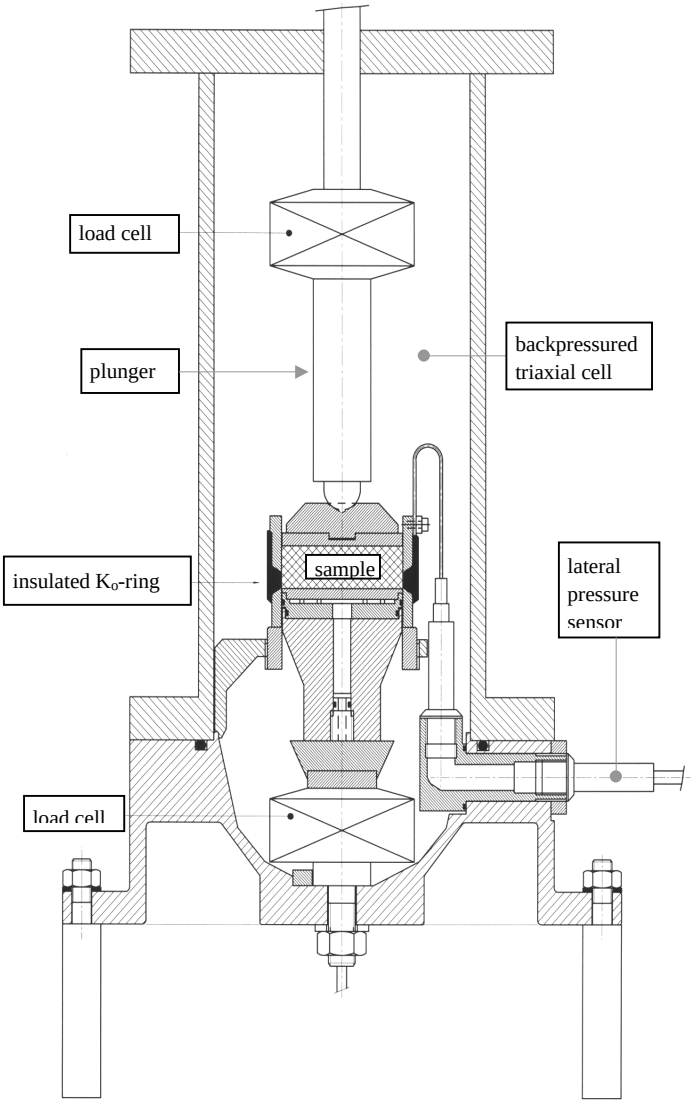

Figure 1 K_o-C.R.S. oedometer

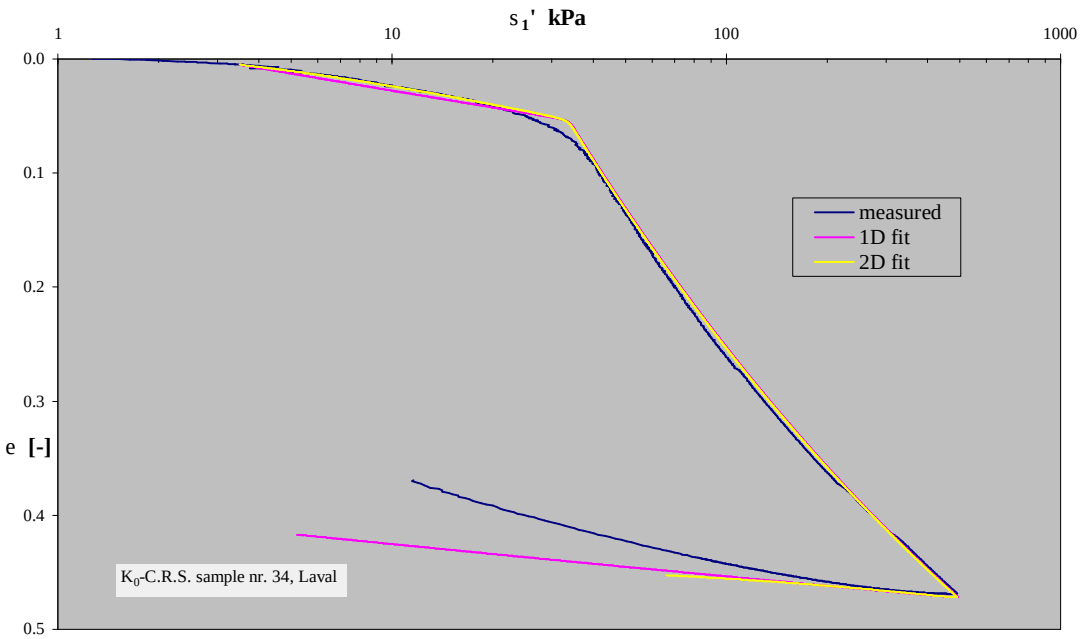

Figure 2 1-D and 2-D model fits of K_o-C.R.S. oedometer test on Oostvaardersplassen clay

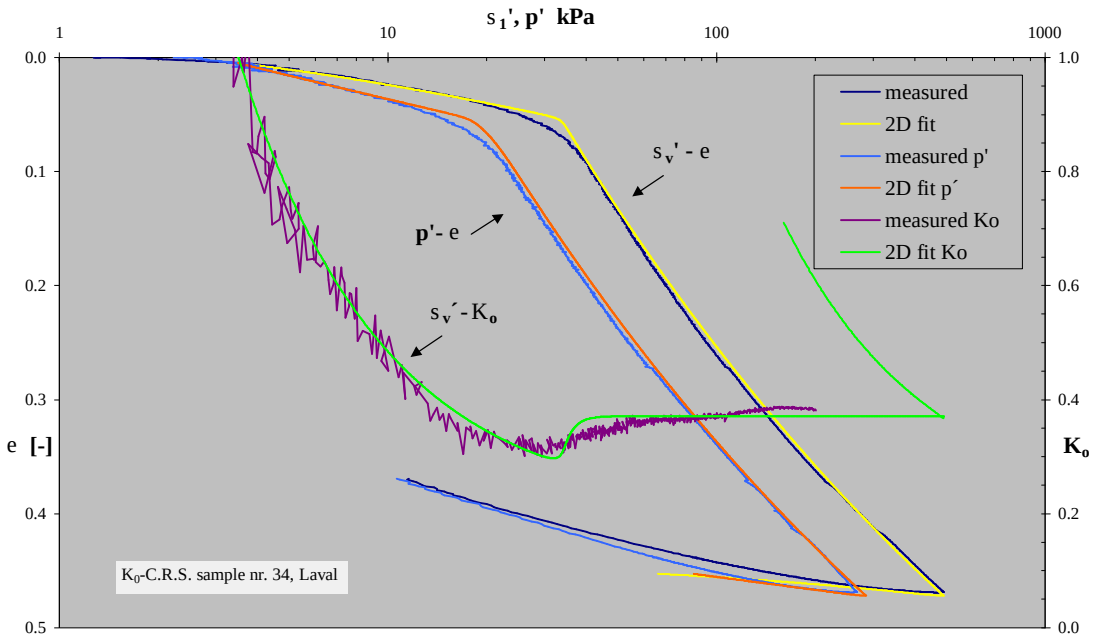

Figure 3 2-D model fits of σ_v', p', ε, K_o for a K_o-C.R.S. oedoemter test on Oostvaardersplassen clay

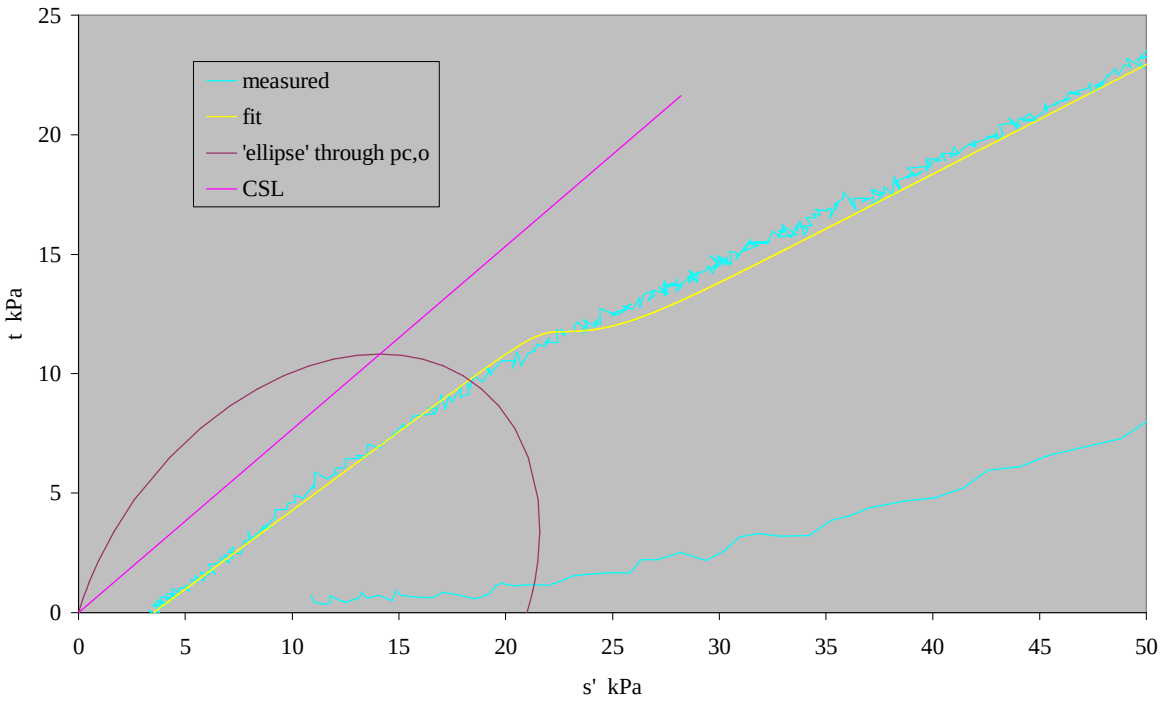

Figure 4 2-D model fits of s' - t for a K_o-C.R.S. oedoemter test on Oostvaardersplassen clay

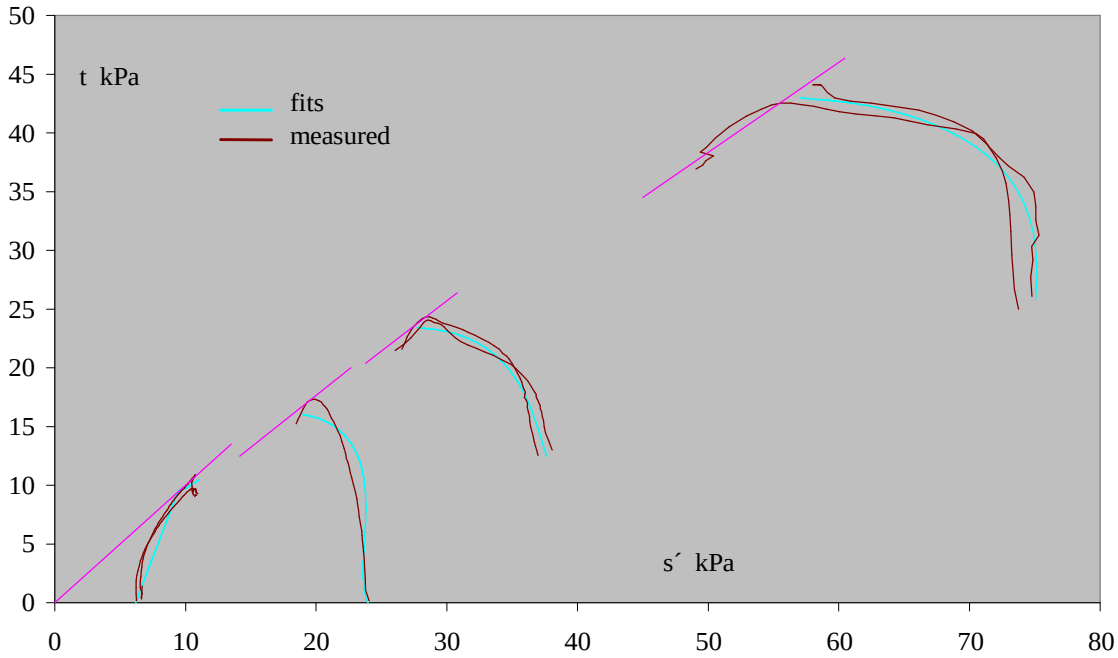

Figure 5 Fits in s' - t space of several triaxial tests on Oostvaardersplassen clay

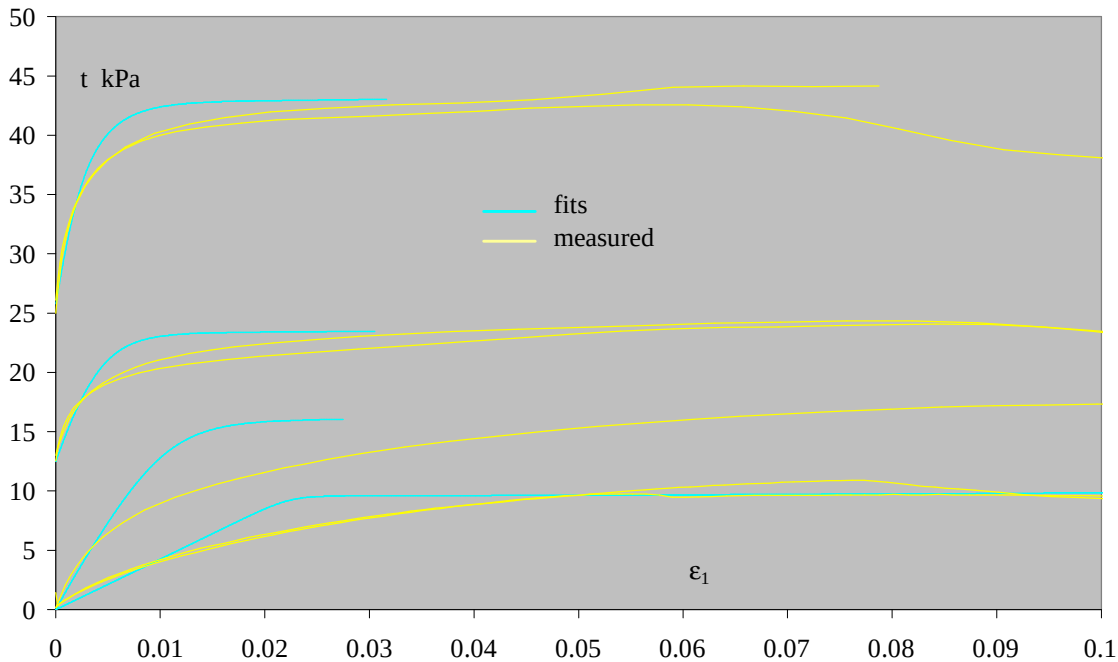

Figure 6 Stress - strain fits of several triaxial tests on Oostvaardersplassen clay

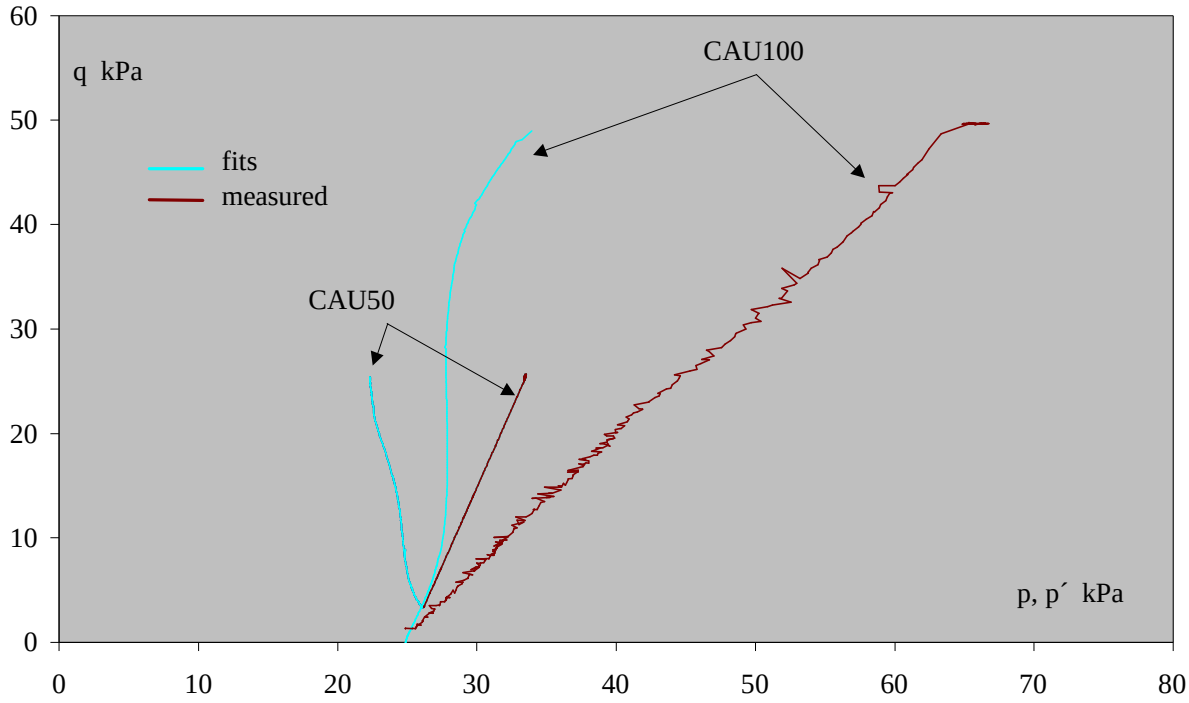

Figure 7 Fits of aniostropic consolidation stages of CAU triaxial tests on Oostvaardersplassen clay

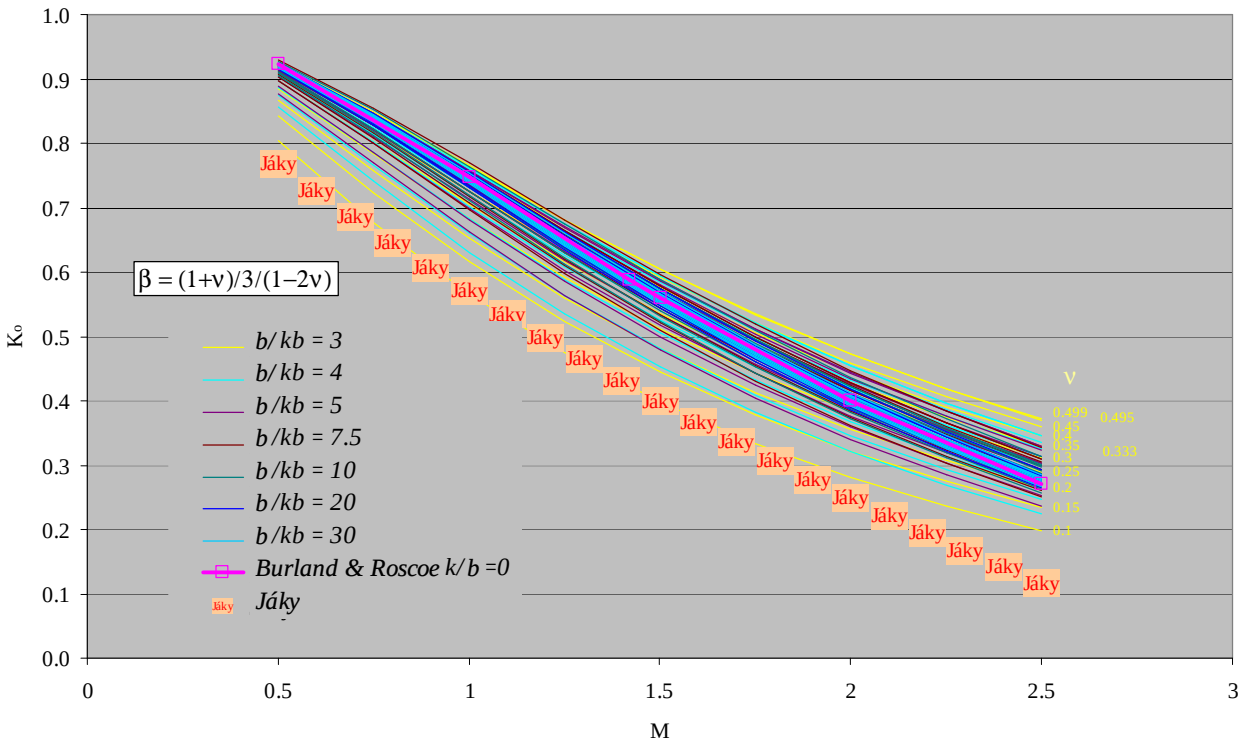

Figure 8 K_o v. M as function of ν and $b/\kappa b$ (or $b/a\ b$), Equation (8.8)

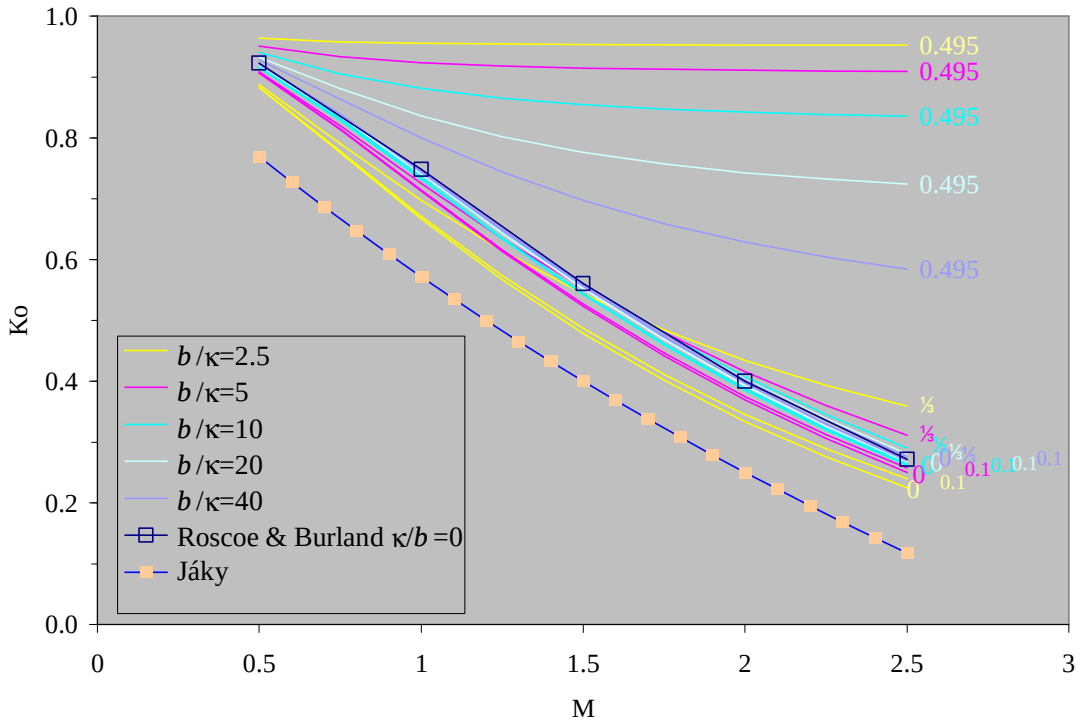

Figure 9 K_o v. M as function of ν and $b/\kappa b$ (or b/a), Equation (8.8)

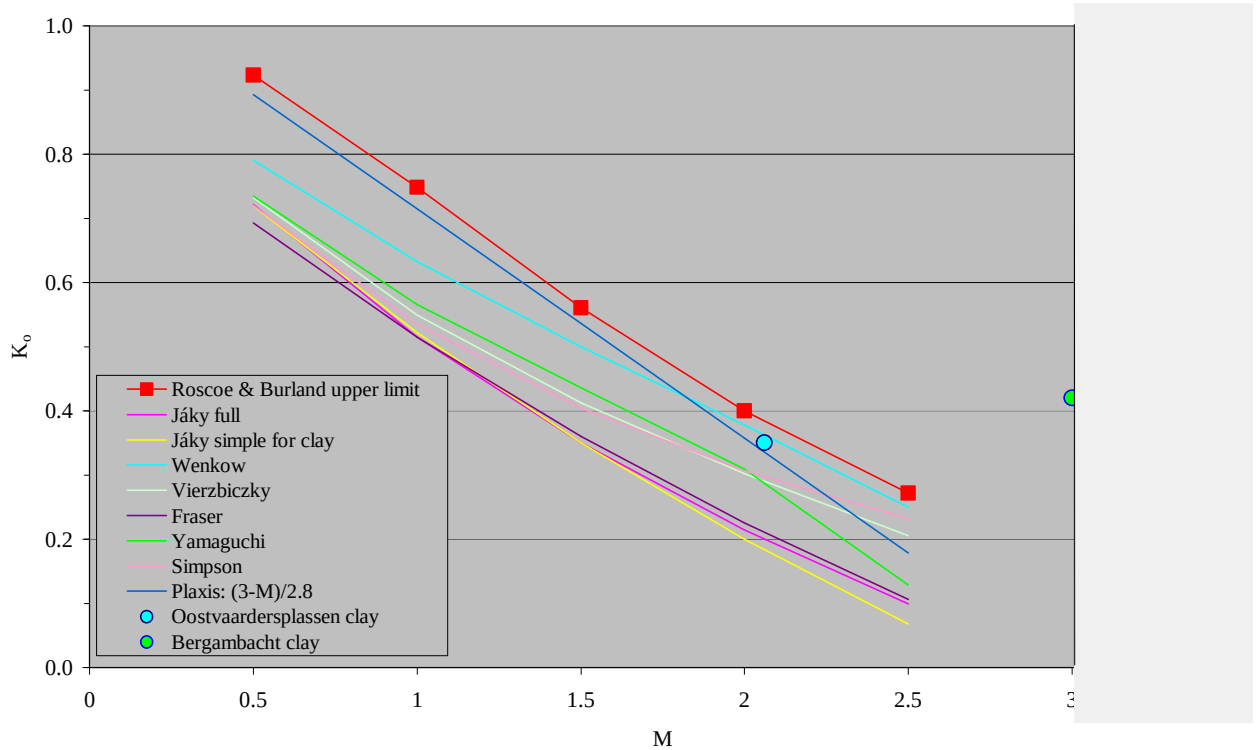

Figure 10 K_o-M correlations from the literature

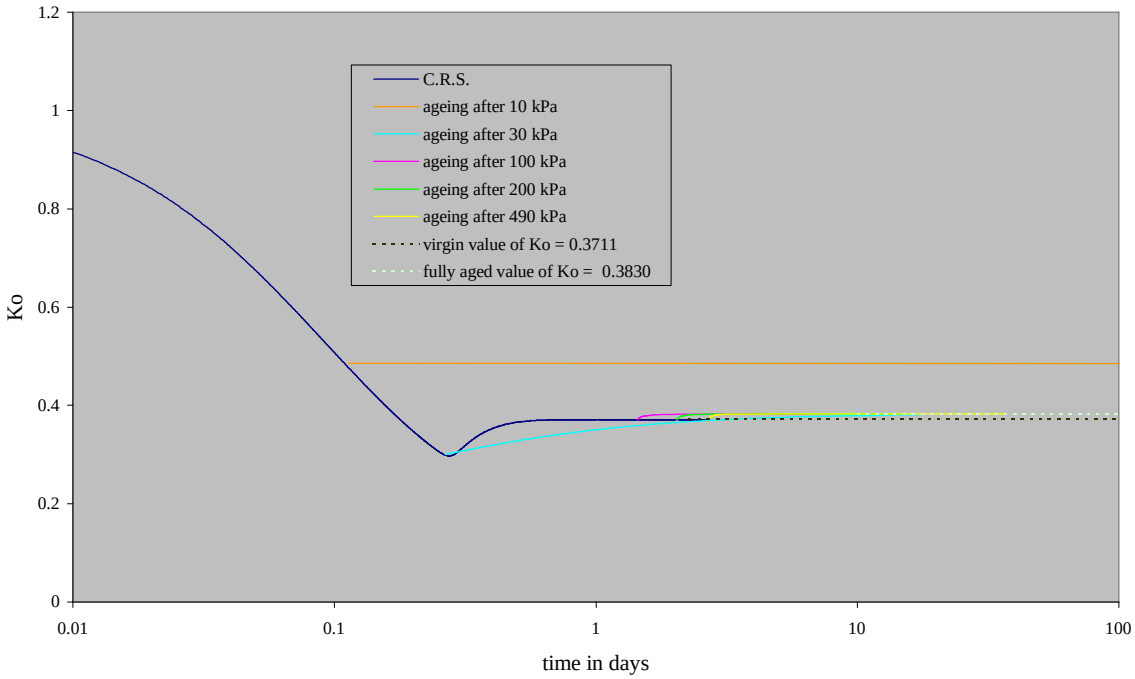

Figure 11 Influence of ageing and OCR on development of K_o

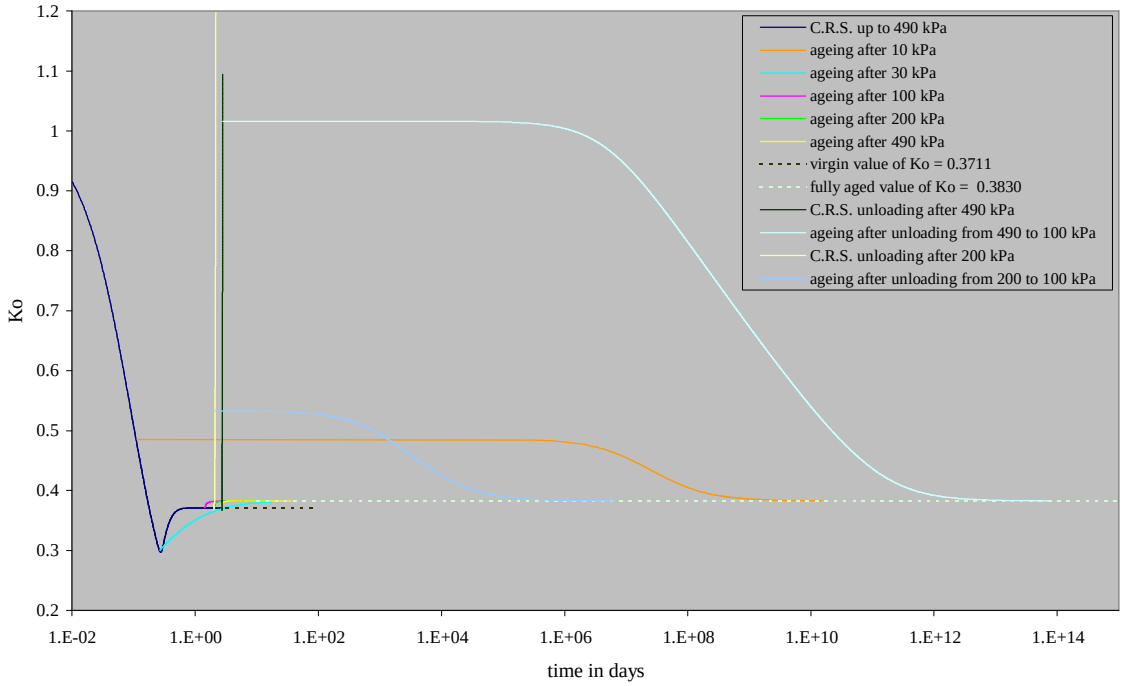

Figure 12 Influence on K_o of unloading followed by creep

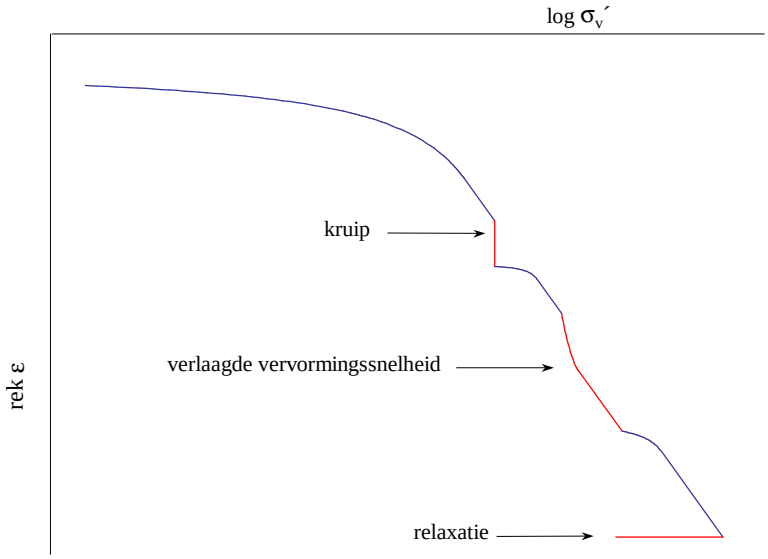

Figure 13 Three methods to generate information on creep properties in a C.R.S. test

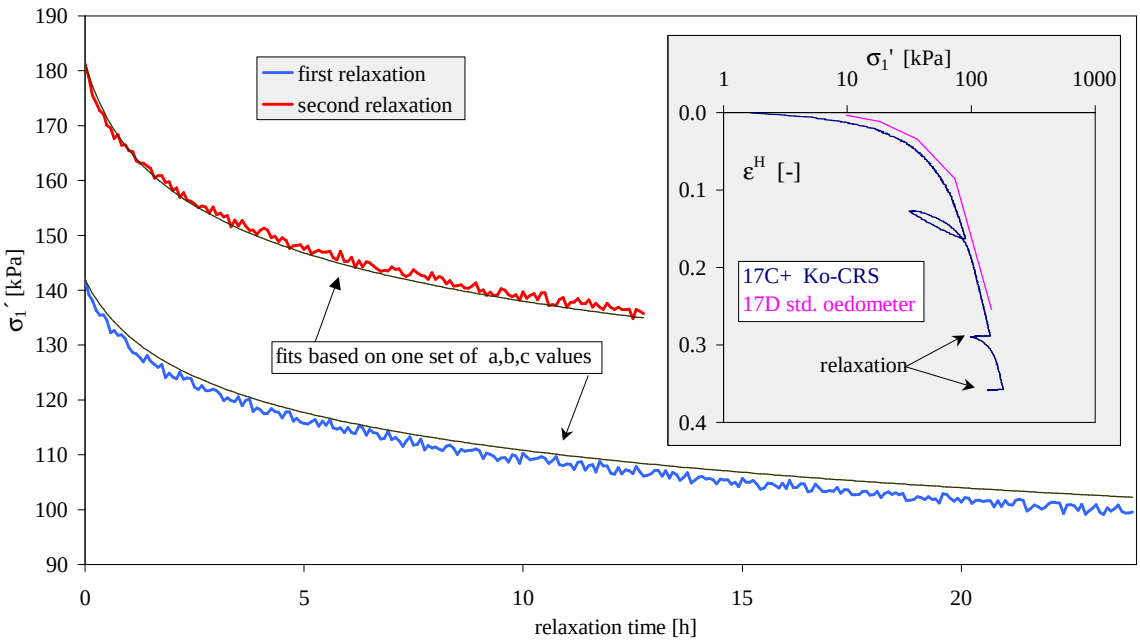

Figure 14 Creep data from relaxation phases in a K_o C.R.S. test

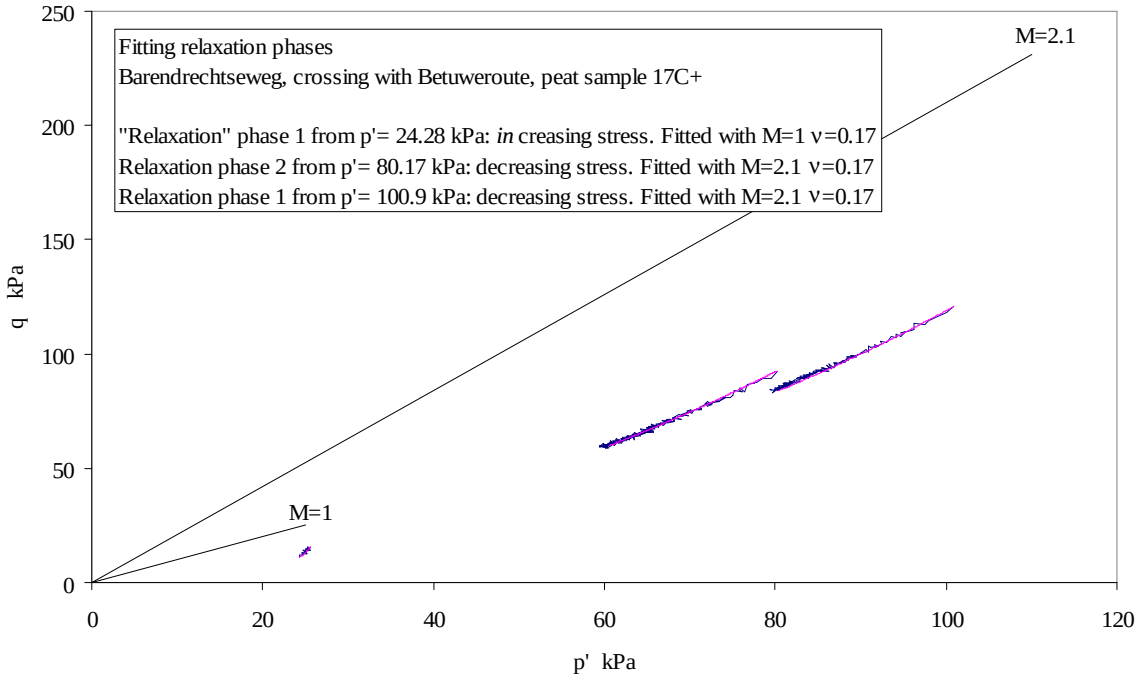

Figure 15 Relaxation phases in K_o-C.R.S. test in q-p': measured data and fits